



Mathematisch-Naturwissenschaftliche Fakultät

Christian M. Wolff | Pietro Caprioglio | Martin Stolterfoht  
Dieter Neher

# Nonradiative Recombination in Perovskite Solar Cells

The Role of Interfaces

Suggested citation referring to the original publication:

Advanced Materials (2019) Art. 1902762

DOI <https://doi.org/10.1002/adma.201902762>

ISSN (print) 1521-4095

ISSN (online) 0935-9648

Postprint archived at the Institutional Repository of the Potsdam University in:

Postprints der Universität Potsdam

Mathematisch-Naturwissenschaftliche Reihe ; 772

ISSN 1866-8372

<https://nbn-resolving.org/urn:nbn:de:kobv:517-opus4-437626>

DOI <https://doi.org/10.25932/publishup-43762>



# Nonradiative Recombination in Perovskite Solar Cells: The Role of Interfaces

Christian M. Wolff,\* Pietro Caprioglio, Martin Stolterfoht,\* and Dieter Neher\*


Perovskite solar cells combine high carrier mobilities with long carrier lifetimes and high radiative efficiencies. Despite this, full devices suffer from significant nonradiative recombination losses, limiting their  $V_{OC}$  to values well below the Shockley–Queisser limit. Here, recent advances in understanding nonradiative recombination in perovskite solar cells from picoseconds to steady state are presented, with an emphasis on the interfaces between the perovskite absorber and the charge transport layers. Quantification of the quasi-Fermi level splitting in perovskite films with and without attached transport layers allows to identify the origin of nonradiative recombination, and to explain the  $V_{OC}$  of operational devices. These measurements prove that in state-of-the-art solar cells, nonradiative recombination at the interfaces between the perovskite and the transport layers is more important than processes in the bulk or at grain boundaries. Optical pump-probe techniques give complementary access to the interfacial recombination pathways and provide quantitative information on transfer rates and recombination velocities. Promising optimization strategies are also highlighted, in particular in view of the role of energy level alignment and the importance of surface passivation. Recent record perovskite solar cells with low nonradiative losses are presented where interfacial recombination is effectively overcome—paving the way to the thermodynamic efficiency limit.

## 1. Introduction

Sustainable and efficient energy production is one of the greatest challenges of humanity in the 21st century. Due to their outstanding optoelectronic and material properties, perovskite solar cells provide a highly efficient and sustainable alternative to fossil fuels and provide an enormous potential to trigger a revolution in power generation for the coming generation. After

C. M. Wolff, P. Caprioglio, Dr. M. Stolterfoht, Prof. D. Neher  
Institute of Physics and Astronomy  
University of Potsdam  
Karl-Liebknecht-Str. 24-25, 14476 Potsdam, Germany  
E-mail: chriwolff@uni-potsdam.de; stolterf@uni-potsdam.de;  
neher@uni-potsdam.de

P. Caprioglio  
Helmholtz-Zentrum Berlin für Materialien und Energie  
Young Investigator Group Perovskite Tandem Solar Cells  
Kekuléstraße 5, 12489 Berlin, Germany

 The ORCID identification number(s) for the author(s) of this article can be found under <https://doi.org/10.1002/adma.201902762>.

© 2019 The Authors. Published by WILEY-VCH Verlag GmbH & Co. KGaA, Weinheim. This is an open access article under the terms of the Creative Commons Attribution License, which permits use, distribution and reproduction in any medium, provided the original work is properly cited.

DOI: 10.1002/adma.201902762

just a few years of research, lead halide perovskite solar cells have reached certified efficiencies of 25.2%, thereby already exceeding other well-established thin film solar cell technologies, such as CIGS or CdTe in small devices (<1 cm<sup>2</sup>).<sup>[1,2]</sup> Considering their nearly ideal optoelectronic properties for a solar cell semiconductor, that is, a high absorption coefficient, long carrier diffusion lengths, and highly luminescent nature, it is expected that perovskites will reach or even surpass the power conversion efficiency (PCE) of monolithic silicon solar cells (26.7%).<sup>[3,4]</sup> Moreover, their comparatively wide bandgap and simple fabrication (from solution or evaporation) render them ideal candidates for applications in silicon-based tandem devices, where the perovskite solar cell is attached as add-on to, for example, industrially fabricated passivated emitter rear contact (PERC) or heterojunction with an intrinsic thin layer (HIT) silicon cells.<sup>[5–7]</sup> Today, silicon/perovskite tandem solar cells have the largest potential for a rapid industrial realization in the near future and sil-

icon/perovskite tandem solar cells with 28.0% PCE have already been demonstrated.<sup>[8]</sup> Importantly, tandem solar cells are not bound to the thermodynamic limitations of single-junction cells and efficiencies beyond 35%<sup>[9]</sup> have been predicted for two- and four-terminal silicon/perovskite tandem cells. In order to unlock these potential PCEs for single-junction and tandem perovskite solar cells, it is essential to gain a more detailed understanding of the underlying recombination loss processes. It is well established that nonradiative recombination losses are the primary reason that perovskite solar cells have not yet achieved their full thermodynamic potential.<sup>[10,11]</sup> Nonradiative recombination losses limit not only the cells' open-circuit voltage ( $V_{OC}$ ) but also the fill factor through an ideality factor larger than one.<sup>[10,12]</sup>

The source of nonradiative recombination losses in perovskite cells remains a heavily debated topic. Historically, the main focus was reducing trap-assisted recombination at defects in the perovskite bulk or at grain boundaries.<sup>[10,13,14]</sup> Indeed, considerable improvements were achieved through advanced perovskite fabrication schemes to increase the grain size, enhance crystallinity, and the invention of multication and/or multihalide formulations. More recently, an increasing number of publications have been dedicated to addressing the issue of recombination at the perovskite surfaces<sup>[15–18]</sup> which differs from the bulk in terms of chemical composition and morphology.<sup>[14,16,19]</sup> For example, Beard and co-workers studied the charge carrier

dynamics in single crystals and polycrystalline thin layers of methylammonium lead iodide/bromide (MAPbI<sub>3</sub>/MAPbBr<sub>3</sub>) using transient reflectance spectroscopy (TRS).<sup>[20,21]</sup> In contrast to the often employed transient absorption spectroscopy (TAS), this technique is very sensitive to the photoinduced carrier concentration in the surface-near region of the semiconductor. Experiments were performed with different excitation energies, thereby varying the penetration depth of the incident light. These investigations showed that surface recombination is more important than recombination within the crystalline grains and at internal grain boundaries. A detailed analysis of the data revealed a surface recombination velocity of less than 10<sup>3</sup> cm s<sup>-1</sup>, orders of magnitude smaller than the recombination velocity of nonpassivated surfaces of traditional semiconductors which are of the order of 10<sup>5</sup> cm s<sup>-1</sup> and above. Interestingly, the MAPI polycrystalline thin layer exhibited longer carrier lifetimes than the corresponding single crystal samples, which was attributed to unintentional trap passivation during thin film preparation. These findings put a strong emphasis on the understanding of the nature of surface traps and the suppression of surface recombination. This is particularly important when considering that advanced perovskites, which comprise multiple anions and/or anions of different chemical nature, are becoming increasingly used throughout the community. Molecular modifiers (e.g., tri-*n*-octylphosphine oxide, TOPO) are often applied to passivate the surface traps. As shown in **Figure 1**, Braly et al.<sup>[22]</sup> recently demonstrated that even the most simple methylammonium lead iodide (MAPI) perovskite absorber (with a bandgap of 1.6 eV) can show an external photoluminescence quantum yield (PLQY) of ≈20%, which would in principle allow a high open-circuit voltage of ≈1.28 V after passivating the top surface with TOPO. This value is very close to the absolute thermodynamic limit of 1.32 V, demonstrating that bulk defects are at least in this case of little importance. Moreover, high external PLQYs were also obtained in other perovskite absorbers (e.g., 66% by Abdi-Jalebi et al.<sup>[23]</sup>). However, the open-circuit voltage of today's perovskite cells barely exceeds 1.2 V<sup>[24–26]</sup> which suggests that significant losses have their origin elsewhere in the multilayer assembly of the device. Recently, significant evidence emerged that main recombination losses in full operational devices originate at or across the interface between the perovskite and charge-transporting layers (CTLs).<sup>[22,27–31]</sup> This will be the major focus of this review.

This progress report consists of four parts: We first focus on the steady-state performance of perovskite solar cells in n-i-p and p-i-n configuration. We discuss several techniques—and their pitfalls—historically used to gain information about the recombination processes in full devices including ideality factor measurements and small-perturbation measurements such as impedance spectroscopy, TPV, and CE. In the second part, we rationalize that absolute photoluminescence measurements on variable layer stacks allow disentangling different recombination pathways. We show that nonradiative recombination has its main origin at the interfaces between the perovskite and the charge-transporting layers, and how these losses depend on the details of the energetics at the hybrid interface. Third, we review work dedicated to establish a fundamental understanding of the microscopic origin of interfacial recombination utilizing techniques with high time resolution. We close by presenting successful pioneering approaches to overcome the limitations



**Christian M. Wolff** is a Ph.D. candidate in the Soft Matter Physics group at the University of Potsdam, Germany. He obtained his master's degree in physics in 2015 from the Ludwig-Maximilians-Universität München, Germany, working on the photophysics and charge carrier dynamics in solar-driven water-splitting semiconductor nanoparticles.

His research interest spans from fundamental semiconductor physics to reducing energy losses in operational perovskite solar cells.



**Martin Stolterfoht** is a postdoctoral researcher in the Soft Matter Physics group at the University of Potsdam, Germany. He completed his master's degree in physics at the University of Graz, Austria in 2012 and obtained his Ph.D. at the University of Queensland, Australia in 2016. His research is focused on providing a fundamental

description of thin-film solar cell operation and charge recombination processes from picoseconds to steady-state through electrooptical measurements and numerical modeling. He also aims at improving perovskite single and multijunction solar cells through the identification and suppression of recombination losses.



**Dieter Neher** is a full-time professor of soft matter physics at the University of Potsdam, Germany. He received his diploma in physics and his Ph.D. in chemical physics at Johannes Gutenberg University in Mainz, Germany. He worked as a postdoctoral research fellow at the Optical Science Center in Tuscon, AZ, and the

CREOL in Orlando, FL, USA. His current research focuses on the understanding and improvement of the electrical and optoelectronic properties of organic conjugated materials, hybrid organic/inorganic systems, and organometallic perovskite semiconductors, and the implementation of such materials into highly efficient devices.

of interfacial recombination and give an outlook on concepts we believe will be the next steps in bringing perovskite solar cells even closer to their thermodynamic limit.

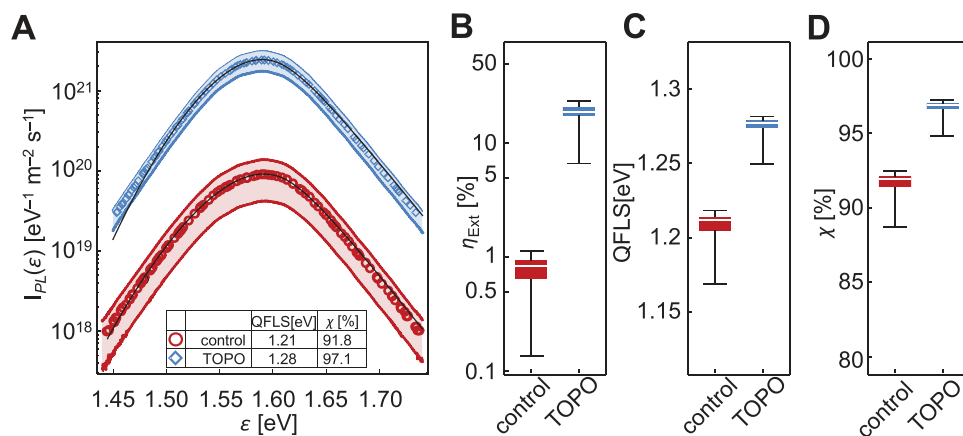


**Figure 1.** A) Absolute intensity photoluminescence spectra of neat  $\text{CH}_3\text{NH}_3\text{PbI}_3$  (MAPI) films with and without TOPO on an Au back-reflector substrate. The black lines are fits to the experimental data (symbols) using the generalized Planck model. B) The external quantum efficiency, C) the quasi-Fermi-level splitting (QFLS), and D) the corresponding fraction of measured quasi-Fermi level splitting versus radiative limit ( $\chi$ ). A–D) Reproduced with permission.<sup>[22]</sup> Copyright 2018, Springer Nature.

## 2. Studies of Steady-State Nonradiative Recombination in Complete Perovskite Solar Cells

Traditionally, information on the steady-state recombination is deduced from measurements on complete solar cells. One popular approach to understand recombination processes in perovskite cells is to measure the ideality factor. Historically, ideality factors were quantified from dark current versus voltage characteristics according to

$$J_{\text{dark}}(V) = J_{\text{R}}(V) = J_0 \cdot e^{\left(\frac{qV}{n_{\text{ID}}k_{\text{B}}T}\right)} \quad (1)$$

with  $q$  the elementary charge,  $V$  the externally applied voltage,  $k_{\text{B}}$  the Boltzmann constant, and  $T$  the temperature. On the other hand, it is common to write the recombination current density  $J_{\text{R}}$  in terms of the carrier density  $n$ :  $J_{\text{R}} \propto n^\alpha$ . Here,  $\alpha$  is the recombination order, which depends on the details of the recombination pathway. For example,  $\alpha = 1$  is realized for ideal trap-assisted recombination through mid-gap impurities,  $\alpha = 2$  for radiative band-to-band recombination of free charges and  $\alpha = 3$  for nonradiative Auger.<sup>[32]</sup> Finally, in the most simple case of an intrinsic semiconductor with sharp band edges, the density of free electrons and holes,  $n$  and  $p$ , is comparably large and proportional to  $e^{\left(\frac{qV}{2k_{\text{B}}T}\right)}$ . This yields the well-known relation between  $n_{\text{ID}}$  and  $\alpha$ :  $n_{\text{ID}} = 2/\alpha$ .<sup>[33]</sup> Interestingly, in perovskite solar cells, the ideality factor varies between  $\approx 1$  and  $2$ ,<sup>[11–13,34]</sup> which has been interpreted in terms of a competition between free carrier recombination and trap-assisted recombination (Shockley–Read–Hall or SRH recombination). For example, measurements of the dark current of p-i-n perovskite devices by Wetzelaer et al.<sup>[35]</sup> yielded a temperature-independent ideality factor of 1.75, though within a small voltage range (0.75–0.9 V). On the other hand, plotting the electroluminescence intensity  $I_{\text{EL}}$  from radiative recombination versus applied voltage yielded a light ideality factor of nearly one. In combination, these observations led to the conclusion that light emission stems from free carrier-band to-band recombination while the total recombination current is

dominated by trap-assisted recombination. However, dark  $J$ - $V$  measurements may be considerably influenced by the shunt resistance at low voltages and the series resistance at high voltages, rendering this method error-prone. A more elegant and already well-established approach in this regard is to cancel the influence of the series resistance by measuring the  $V_{\text{OC}}$  as a function of the light intensity  $I$  (or the generation current density  $J_{\text{C}}$ ) according to<sup>[36]</sup>

$$J_{\text{light}}(V = V_{\text{OC}}) = J_0 \cdot \left[ e^{\left(\frac{qV_{\text{OC}}}{n_{\text{ID}}k_{\text{B}}T}\right)} - 1 \right] - J_{\text{C}}(I) = 0 \quad (2)$$

Since there is no current flowing at  $V_{\text{OC}}$ , the series resistance becomes irrelevant and the obtained ideality factor is only dependent on the (internal) recombination pathways and the shunt which can be however readily identified and disregarded in the analysis. Using this approach, Tress obtained an ideality factor of  $\approx 1.6$  in the relevant intensity regime in efficient n-i-p cells based on planar  $\text{SnO}_2$  or mesoporous  $\text{TiO}_2$  and concluded that this value is a result of distributed SRH recombination via bulk defects (Figure 2).<sup>[13]</sup> Moreover, for an aged cell, an ideality factor close to 2 was interpreted to be a consequence of increased SRH recombination, due to a large increase in bulk defects. However, in samples without hole transport layer (HTL), where the perovskite was in direct contact to the metallic Au electrode, the ideality factor was close to 1 which could be easily misinterpreted as dominant free carrier radiative recombination. Such a scenario would, however, give rise to a high photoluminescence quantum efficiency, which is a very rare case for complete perovskite device stacks (see above). Instead, a detailed analysis of the data revealed surface recombination as the major loss process. Strong surface recombination for both types of carriers would even allow for ideality factors  $< 1$ , that is, the  $V_{\text{OC}}$  saturates and cannot be increased with higher illumination intensity. This was shown, for example, by Tvingstedt et al.<sup>[34]</sup> In line with this interpretation, measurements in p-i-n type solar cells with unmodified (semimetallic) poly(3,4-ethylenedioxythiophene):polystyrene sulfonate (PEDOT:PSS) as HTL exhibited an ideality factor close to 1.<sup>[37]</sup>

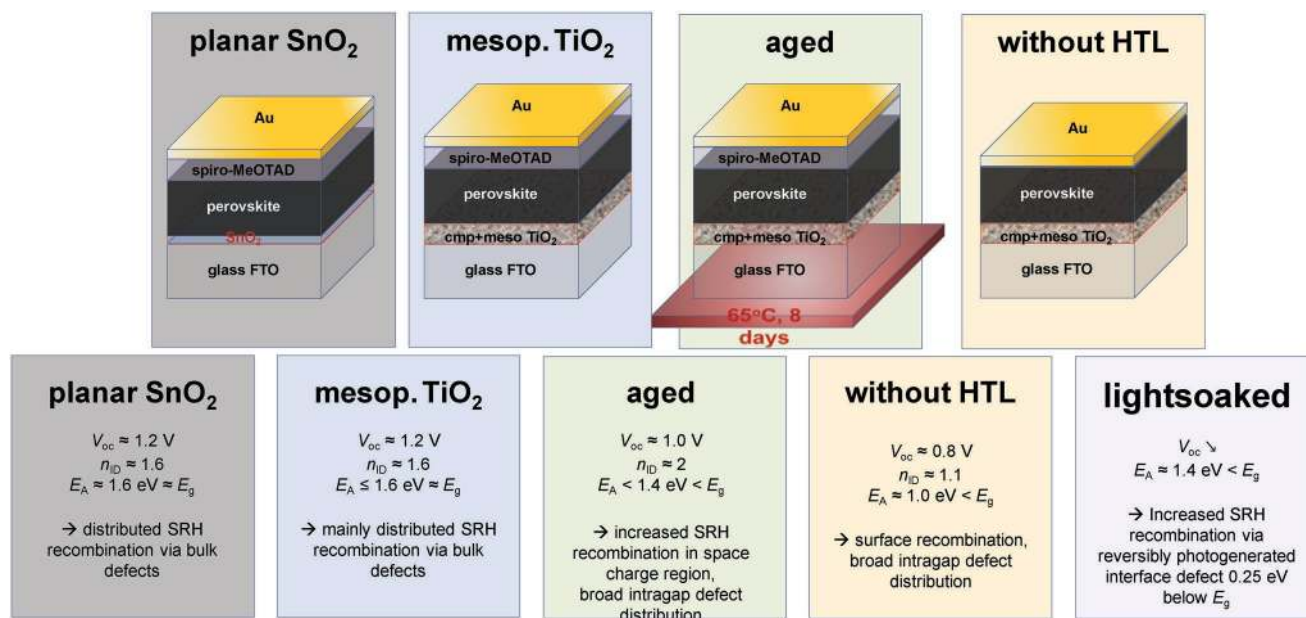


**Figure 2.** Ideality factors and attributed recombination mechanism in n-i-p cells with different electron transport layers (SnO<sub>2</sub> and TiO<sub>2</sub>), an aged device (based on TiO<sub>2</sub>, kept 8 d under 1 sun white-light LED illumination at 65 °C in N<sub>2</sub>), a device without HTL and a light-soaked device (1 sun equivalent illumination for 80 min at open-circuit). Adapted with permission.<sup>[13]</sup> Copyright 2018, Royal Society of Chemistry.

The above findings and interpretations point to the difficulty in assigning a measured value of  $n_{ID}$  to a specific recombination process. Moreover, the above relations assume that the densities of electrons and holes are comparable and homogeneous throughout the active layer. Consider, for example, radiative band-to-band recombination. Here, the local rate  $R(x)$  depends on the local densities of electrons and holes via  $R(x) = k_2 n(x)p(x)$ . Charge injection from ohmic contacts, selective trapping, the attachment of charge-transporting layers and electrodes, etc., can result in a large variation of the carrier concentrations across the active layer thickness but also give rise to imbalanced electron and hole densities even at  $V_{oc}$ .<sup>[38–42]</sup> In such a case, the ideality factor does not necessarily reflect the order of the predominant recombination process.<sup>[33]</sup>

Recently, Bongiovanni and co-workers pointed out that electrons and holes may even have different recombination orders. In this case,  $n_{ID} = \left(\frac{1}{\alpha_e} + \frac{1}{\alpha_h}\right)$ , where  $\alpha_e$  and  $\alpha_h$  are the individual recombination order ( $\alpha_{e/h} = 1, 2, 3$ ; see above) for electrons and holes, respectively.<sup>[43]</sup> They considered a trap-assisted recombination process, where the first step is the capture of electrons by a trap, followed by the recombination of a free hole by the trapped electron. If the trap is situated such that the fraction of occupied traps is small, the rate of free electron capture is proportional to its density and  $\alpha_e = 1$ . Holes, on the other hand, recombine in a bimolecular fashion with trapped electrons, whose density  $n_T$  is proportional to  $p$ , resulting in  $\alpha_p = 2$ . In combination, this picture leads to  $n_{ID} \approx 1.5$ , a frequently reported value for perovskite solar cells. This approach, therefore, provides a potential explanation for the observation that recombination is mostly nonradiative but that the ideality factor differs significantly from the prediction of SRH recombination, where  $n_{ID} \approx 2$ .

However, in addition,  $n_{ID}$  will depend on the exact *shape* of the density of states distribution through which recombination proceeds.<sup>[44,45]</sup> For example, for an exponential band tail,  $n \propto e^{\left(\frac{qV}{m k_B T}\right)}$ , where  $m$  is a parameter describing the width of the tail, this results in  $n_{ID} = m/\alpha$  for the most simple case of similar band tails for electrons and holes. The situation becomes even more complicated when considering the exact recombination pathway, for example, trapped with free carriers, free with free carriers, or different shapes of the DOS of electrons and holes near the band-edge.<sup>[45]</sup> This renders it even more challenging to interpret the value of  $n_{ID}$  in terms of the predominant recombination mechanism without additional information on the details of the recombination pathways and the energetic and spatial distribution of carriers. This conclusion is particularly important in view of the complex multilayer architecture of perovskite solar cells, where recombination is not restricted to the bulk of the perovskite layer and carrier distributions are influenced by the dynamic equilibrium of extraction, reinjection, and recombination mediated by the CTLs. Furthermore, slow dynamic processes that depend, for example, on ionic movement,<sup>[46]</sup> which itself depends on a manifold of parameters such as processing conditions, dielectric constants, or doping of the CTLs, complicate the information one can draw from this “figure-of-merit.” For example, Calado et al.<sup>[47]</sup> nicely showed that the ideality factor can take any value between 1 and 2 in the same device, depending on prebiasing condition and settling time of the measurement, typically not reported, but—bearing these results in mind—should be.

Alternative to these “steady-state” measurements, small-perturbation techniques such as impedance spectroscopy (IS),<sup>[48–51]</sup> and transient photovoltage measurements (TPV)<sup>[27,52]</sup> in combination with differential charging (DC)<sup>[53]</sup> have been

extensively applied to perovskite solar cells in order to provide a comprehensive picture of the recombination in full devices. In IS, the solar cell is held under steady-state illumination with a set intensity, while the external bias is modulated around a given DC bias. This causes a periodic variation of the current which is recorded as a function of the modulation frequency. While IS has the advantage that it can be easily performed with a commercially available impedance spectrometer, the analysis of the data requires to “simplify” the device by an equivalent circuit, which is not a trivial task.<sup>[54]</sup> For example, Zarazua et al.<sup>[49]</sup> performed IS measurements on n-i-p perovskite solar cells for different illumination intensities and perovskite thicknesses. The analysis of the data with an equivalent circuit with two capacitors and three resistors revealed two regimes, a high-frequency regime assigned to processes in the bulk and a low-frequency regime associated to interfacial charge accumulation and recombination. The detailed analysis led to the conclusion that the steady-state response of these cells is mainly determined by the charge carrier kinetics at the surfaces, while processes in the bulk are of minor importance. Recombination times from this study were, however, in the range of 1 ms to 1 s, which is several orders larger than charge carrier decay times deduced from TPV or PL measurements (see next). One difficulty in analyzing IS data comes from the motion of ions in response to the alternating voltage, meaning that the low-frequency response of the cell may reveal the combined properties of ions, electrons, and holes.<sup>[54]</sup>

TPV records the dynamics of the  $V_{OC}$  drop of a cell after it has been exposed to a short laser pulse. In most cases, the sample is held at a given  $V_{OC}$  by illuminating the sample with a given steady state illumination intensity and by using a large output resistor. Exposing the sample to a short laser pulse of low fluence causes a small perturbation from quasi-equilibrium, expressed by a sudden increase of the  $V_{OC}$ . The transient decay of  $V_{OC}$  back to its stationary value is analyzed in terms of the charge carrier dynamics. **Figure 3** summarizes the results from such a study, where TPV and DC were applied to p-i-n cells. Here, the bandgap of the perovskite was enlarged by increasing the concentration of Br in the mixed  $\text{CH}_3\text{NH}_3\text{Pb}(\text{I}_{1-x}\text{Br}_x)$  perovskite. PEDOT:PSS served as the HTL while either phenyl-C61-butyric acid methyl ester (PCBM) or PCBM blended with 20% of the higher adduct fullerene ICBA was used as the electron-transport layer (ETL). As shown in **Figure 3a**, the  $V_{OC}$  was affected by both the composition of the perovskite and the choice of the ETL, along with distinct changes of the carrier concentration at a given steady-state illumination intensity (from DC) and carrier lifetime (from TPV). Increasing the Br-content increased the  $V_{OC}$  but reduced the carrier lifetime, while the addition of the ICBA was beneficial for both properties. A detailed analysis of the data revealed the existence of an exponential tail of defect states, which serve as recombination centers. Interestingly, the ideality factor of the sample with a 20% Br content and a PCBM ETL was below one at higher light intensities, indicating failing contact selectivity, which may also diminish the carrier lifetime. Following this line of arguments, the addition of ICBA to the ETL was proposed to reduce the impact of recombination at the perovskite/PCBM interface, which was attributed to a different interface energetics as discussed in greater detail next.

It has been pointed out that carrier lifetimes measured via TPV may be affected by capacitive effects.<sup>[55]</sup> More recently, Kiermasch et al. provided further guidance under which conditions measured carrier lifetimes may not be influenced by the capacitive discharge,<sup>[52]</sup> which allows quantifying true lifetimes in perovskite solar cells. Measurements on samples with “sufficiently” thick perovskite layers and high enough carrier densities were interpreted in terms of bulk recombination with a recombination order of 1.6–2. Notably, the analysis of the data yielded a disorder factor  $m$  of 2.8, again indicating a significant exponential broadening of the sites involved in the recombination process. This finding seems at variance with the very sharp absorption onsets of typical perovskite absorbers, and suggest that such states are *dark* (they do not contribute to the optical absorption and radiative recombination). However, DC measures only the average carrier density, while the recombination properties are depending on the spatial distributions of the photogenerated excess carriers as pointed out above. Notably, the attachment of a selective CTL (which specifically extracts only one type of carrier while blocking the other) introduces very inhomogeneous carrier profiles. Charge carrier lifetimes as deduced from TPV measurements range typically between few hundreds of nanosecond to several microseconds, depending on the sample layout and the illumination intensity. Such values seem reasonable in the view of significant nonradiative  $V_{OC}$  losses in these devices. Discrepancies of “carrier lifetimes” between measurements with different techniques including electrical such as impedance or capacitance measurements, electrooptical such as OTRACE,<sup>[56]</sup> TPV or TDCF,<sup>[57]</sup> and finally all-optical such as transient photoluminescence (TRPL), TAS, TRS, or microwave conductivity (TRMC) and optical pump terahertz probe (OPTP)<sup>[58]</sup> call for comparative examination of the different techniques. Particular care should be taken regarding several parameters which may influence the result. These include the excitation condition (excitation wavelength,<sup>[59,60]</sup> repetition rates,<sup>[61]</sup> and intensities), the setup time resolution (resistance–capacitance limitation), and the “sample-history”<sup>[62]</sup> (e.g., measuring from high-to-low intensity or vice versa). Moreover, it is clear that very different processes happen on different timescales, that is, carrier-cooling, carrier-trapping, carrier-extraction on ps timescales; carrier-motion, carrier-detraping, carrier-recombination, and electrode charge-up on ns-to- $\mu$ s-timescales; and finally ionic movement, (electro-)chemistry at the electrodes, in the bulk or at CTLs on ms timescales and above.

### 3. Pinpointing the Origin of Nonradiative Recombination in Perovskite Multilayer Stacks Using Absolute PL Measurements

A disadvantage of the above-mentioned electrical and electrooptical methods is that they require complete solar cells. This renders it difficult to pinpoint or locate the origin of the nonradiative losses in the multilayer system as recombination through different channels occurs in parallel.<sup>[31]</sup> This problem can be circumvented when probing the density and fate of carriers with all-optical techniques, for example, by studying the

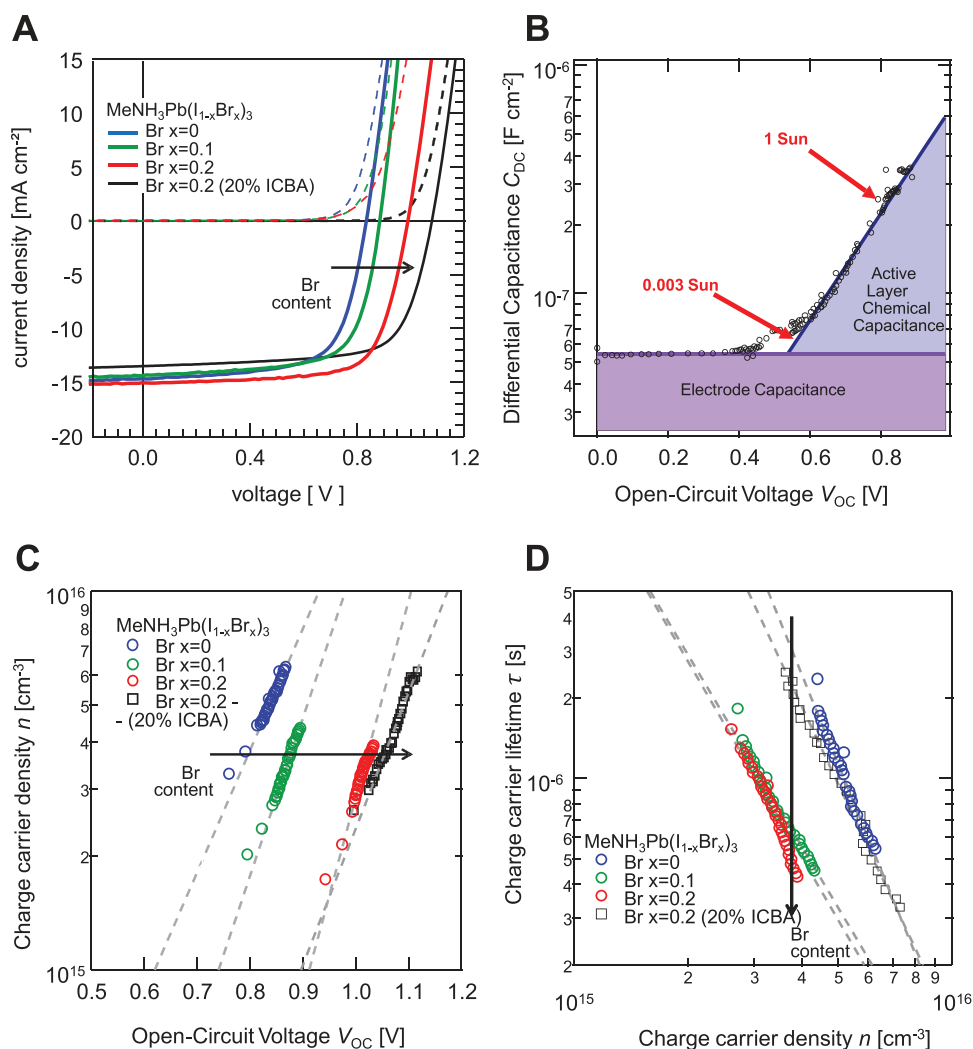


**Figure 3.** Results from transient optoelectronic measurements on p-i-n solar cells, comprising a mixed  $\text{CH}_3\text{NH}_3\text{Pb}(\text{I}_{1-x}\text{Br}_x)_3$  perovskite sandwiched between a PEDOT:PSS hole transporting layer and a PCBM electron transporting layer to which ICBA was also added in one case. A) The addition of Br to the perovskite and of ICBA to the ETL both increase the  $V_{\text{OC}}$ . B) Differential charging indicates that most photogenerated charges reside in the active layer under application-relevant illumination conditions. C, D) Despite similar effects on the  $V_{\text{OC}}$ , the addition of Br and ICBA changes the carrier concentration and the carrier lifetime in different ways, pointing to the interplay between bulk and interface recombination. A–D) Adapted with permission.<sup>[53]</sup> Copyright 2017, American Chemical Society.

(temporal change in) absorption/reflectance or luminescence upon illumination.

In this spirit, we and others utilized measurements of the absolute intensity of the emitted PL ( $\phi_{\text{PL}}$ ) to analyze the steady-state recombination losses in (perovskite) thin films and solar cells.<sup>[43,63–65]</sup> The strategic advantage of these measurements is that it can be performed on any layer assembly, with and without the presence of CTLs or electrodes. Also, if PL experiments are performed in steady state in the absence of electrodes or at  $V_{\text{OC}}$ , the emitted photon flux under illumination with a given intensity yields the absolute radiative and nonradiative recombination currents. This is a decisive advantage over other techniques when trying to assess nonradiative recombination in perovskite films. Moreover, the absolute emitted PL—or equivalently the radiative recombination current density ( $J_{\text{rad}} = \phi_{\text{PL}}/e$ )—is a direct measure of the chemical

potential per free electron–hole pair ( $\mu$ ) or the quasi-Fermi level splitting (QFLS) in the active material<sup>[11,23,43,64,66]</sup>

$$e\phi_{\text{PL}} = J_{\text{rad}} = J_{0,\text{rad}} \cdot e^{(\mu/k_{\text{B}}T)} \quad (3)$$

In Equation (3),  $J_{0,\text{rad}}$  is the radiative thermal recombination current density in the dark. We note that Equation (3) is a simplification of Würfel's generalized Planck law which is only valid for a QFLS a few  $k_{\text{B}}T$  smaller than the bandgap  $\mu < E_{\text{G}} - 3k_{\text{B}}T$ .<sup>[67]</sup> If, on the other hand, all absorbed photons generate free charges, and all photon emission stems from the recombination of free electron–hole pairs, QFLS can be related to the photoluminescence quantum efficiency of the active layer (PLQY) according to

$$\mu = k_{\text{B}} T \ln(\text{PLQY} \cdot J_{\text{G}}/J_{0,\text{rad}}) \quad (4)$$



Equations (3) and (4) are valid if the spectral dependence of  $J_{\text{rad}}$  is identical to  $J_{0,\text{rad}}$ , meaning recombination goes through the same channels regardless of the QFLS. In the case of electrically injected charges, Equation (4) can be varied by exchanging  $\mu$  with  $eV_{\text{OC}}$  and PLQY by the electroluminescence quantum efficiency ( $\text{EQE}_{\text{EL}}$ ), named Rau's reciprocity relation.<sup>[68]</sup> This exchange holds true for equivalent injection and extraction efficiencies (Donolato theorem<sup>[69,70]</sup>). The high photovoltaic external quantum efficiencies ( $\text{EQE}_{\text{PV}}$ ) of perovskite solar cells suggest that extraction and injection are indeed very efficient. Based on these basic considerations, Sarritzu et al.<sup>[43]</sup> proposed to decouple the contributions of bulk and interfacial recombination currents in n-i-p-type perovskite solar cells through the measurement of the QFLS in the individual layers of the cells, that is, the perovskite on glass with and without attached transport layers. The authors found that the attachment of an ETL/HTL to the perovskite resulted in a substantial reduction of QFLS and with that the maximum achievable  $V_{\text{OC}}$  by several tens to hundreds of meV.<sup>[43]</sup> Figure 4a shows that the QFLS of the neat perovskite is larger than the QFLS of the  $\text{TiO}_2$ /perovskite film, the perovskite/Spiro-OMeTAD film and the n-i-p stack which had the lowest QFLS. The authors concluded that nonradiative recombination proceeds mostly at or across the perovskite/CTL interfaces, meaning that the interfacial recombination currents set the largest limitation on the  $V_{\text{OC}}$  and the performance of their cells, see Figure 4b. Wu et al.<sup>[65]</sup> further extended this approach by measuring the intensity dependence of the QFLS<sup>[41]</sup> which allowed the authors to obtain pseudo- $J$ - $V$  curves of the perovskite absorber layer with and without transport layers or electrodes. This powerful approach enables to quantify the impact of nonradiative interfacial recombination not only on the  $V_{\text{OC}}$  but also on the fill factor.

More recently, we used hyperspectral PL imaging (2D maps with coordinates  $[x, y, I_{\text{PL}}(\lambda)]$ ) to pinpoint the origin of

nonradiative recombination losses in p-i-n-type perovskite solar cells with the architecture ITO/PTAA/perovskite/ $\text{C}_{60}$ /BCP/Cu. Measurement of the depth-averaged absolute PL yield ( $I_{\text{PL}}$ ) enabled the creation of 2D QFLS maps<sup>[64,66]</sup> (pixel size:  $10 \times 10 \mu\text{m}^2$ ) on perovskite film with and without attached transport layers as shown in Figure 5.<sup>[11]</sup> On the neat perovskite an average QFLS of 1.21 eV was obtained which was significantly below the radiative limit (1.34 eV). Addition of PTAA (1.125 eV) or  $\text{C}_{60}$  (1.13 eV) lowered the QFLS considerably, however, in contrast to Sarritzu et al., the QFLS of the p-i-n stack was only slightly lower (1.12 eV) compared to the bilayers. This result would be consistent with the expectation that the recombination currents at the bottom and top interface are superimposed in the p-i-n stack, yet both recombination currents lower the QFLS only via the logarithm (see further below). Inserting ultrathin interlayers (PFN-Br and LiF) allowed a substantial reduction of interface-induced recombination losses at both interfaces which increased the  $V_{\text{OC}}$  of the optimized cells to 1.17 V. These improvements enabled p-i-n-type solar cells with efficiencies of 21.6% on small areas and a stabilized certified PCE of 19.83% for a  $1 \text{ cm}^2$  perovskite solar cell. We note that the  $V_{\text{OC}}$  of both the *unoptimized* and the *optimized* cell [ITO/PTAA/(PFN-Br)/perovskite/(LiF)/ $\text{C}_{60}$ ] was identical to the QFLS of the corresponding p-i-n stacks on glass which will be discussed in more detail further below. The study also included a direct comparison between absolute PL and TRPL measurements, which revealed a concurrent increase of the TRPL decay time and the PL yield with reducing interfacial recombination. Interestingly, the monoexponential TRPL lifetime of the neat perovskite film ( $\approx 500 \text{ ns}$ ) and the optimized p-i-n stack ( $\approx 200 \text{ ns}$ ) allows to analytically predict the corresponding QFLS of the neat perovskite film (1.21 eV) and the optimized p-i-n stack (1.17 eV) considering dominant first-order recombination at  $V_{\text{OC}}$ .<sup>[10]</sup> Moreover, through quantification of the

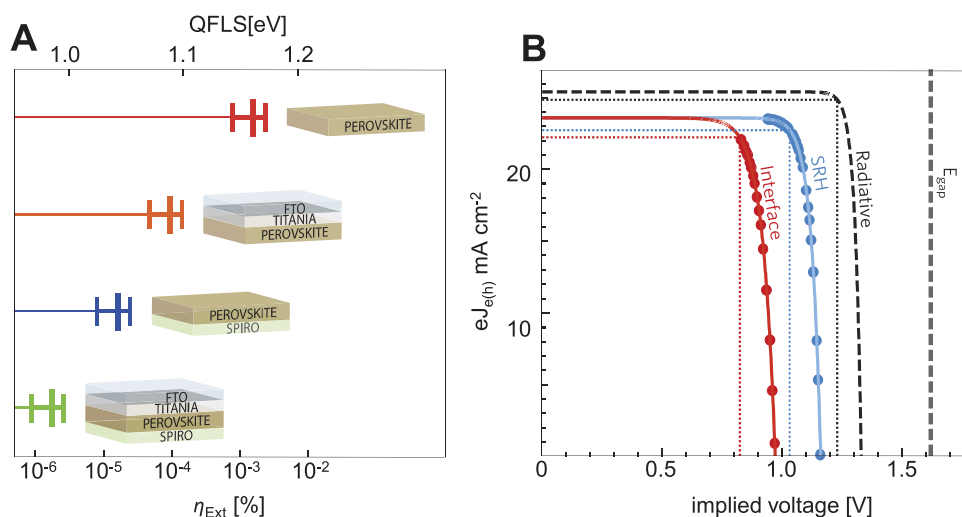


**Figure 4.** A) Comparison of the free electron–hole energy (top axis) and external photoluminescence quantum yield (bottom axis) in neat perovskite with and without attached transport layers under a 1 sun equivalent CW laser excitation at 532 nm ( $50 \text{ mW cm}^{-2}$ ). Substantial interfacial recombination losses were obtained in the presence of the interlayers. B) Predicted  $J$ - $V$  curves, that is, external electron and hole currents that equal the generation current  $J_G$  and the total recombination current  $J_{e/h} = J_G - J_R = J_0 \exp(\mu/n_{\text{D}}k_{\text{B}}T)$  which were calculated based on the experimentally measured ideality factors ( $n_{\text{D}}$ ) on the neat perovskite layer and the n-i-p stack. A,B) Adapted under the terms of the CC-BY Creative Commons Attribution 4.0 International License (<http://creativecommons.org/licenses/by/4.0/>).<sup>[43]</sup> Copyright 2017, The Authors, published by Springer Nature.

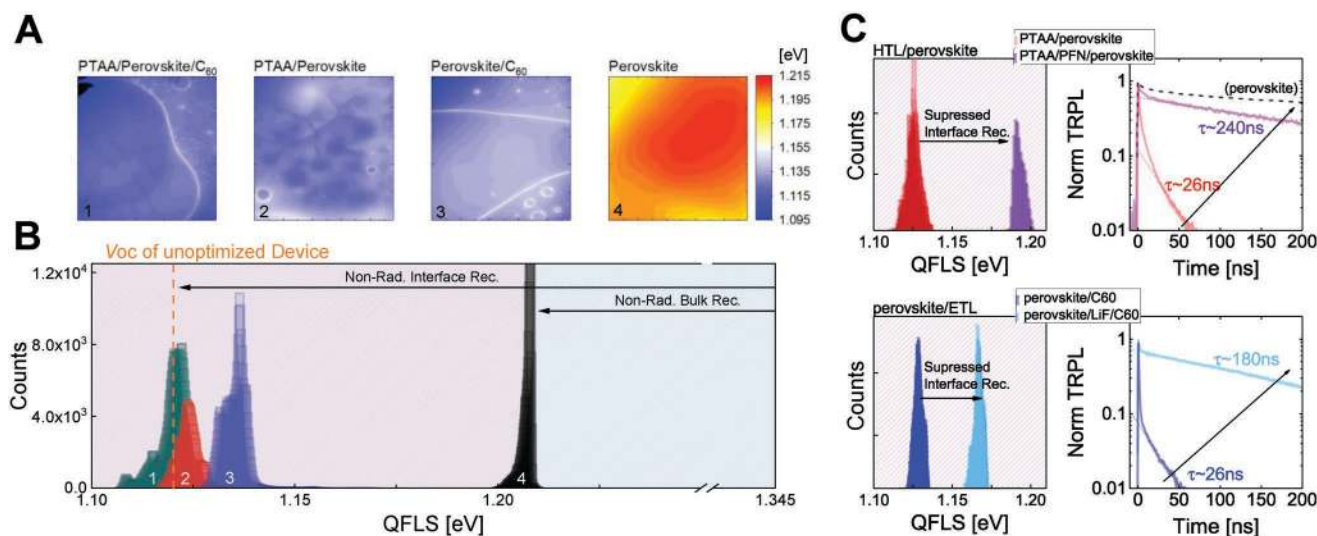


**Figure 5.** A) Hyperspectral QFLS maps ( $1 \times 1 \text{ cm}^2$ ) of the neat perovskite and in conjunction with different CTLs providing information on interfacial and defect recombination in the bulk and the interfaces. B) The QFLS distribution as obtained from the maps shown in (A). Films with transport layers attached to the perovskite exhibit a significantly lower QFLS due to large nonradiative interfacial recombination losses. C) The improvement in QFLS upon inserting additional interfacial layers resulted in a substantial and concurrent increase in QFLS and TRPL lifetime. A–C) Reproduced with permission.<sup>[11]</sup> Copyright 2018, Springer Nature.

interface recombination velocity  $S$ , the  $V_{OC}$  of the *unoptimized* and *optimized* cell could be accurately reproduced numerically. These results suggested that the TRPL decays were dominated by interfacial recombination rather than the transfer of photo-generated carriers to the transport layers, although this may depend on the exact measurement conditions as we discuss further next.

More recently, we generalized this approach to all major perovskite solar cell architectures, including: (1) planar p-i-n-type cells, (2) mesoporous, and (3) planar n-i-p-type cells. This included the study of triple cation perovskite cells and other perovskite compositions<sup>[31]</sup> with ten different CTLs (see **Figure 6**) including conjugated polymers, small molecules, fullerenes, and metal oxides ( $\text{SnO}_2$  and  $\text{TiO}_2$ ). For most studied CTL, it was found that the interfacial recombination current outweighs the recombination current through defects in the neat perovskite (Figure 6). The best transport layers in this study were PTAA/PFN-Br and polyTPD/PFN-Br and  $\text{SnO}_2$  which allowed a QFLS close to the neat perovskite. Among CTL on top of the perovskite, Spiro-OMeTAD was found to be superior to PCBM and  $\text{C}_{60}$  which might be one reason why n-i-p-type cells have historically delivered higher  $V_{OC}$ 's compared to p-i-n-type cells (with few recent exceptions<sup>[24,71–73]</sup>). At this stage we want to emphasize that the myriad of explored and unexplored combinations<sup>[74]</sup> that can be obtained by alloying and mixing any of the three components (A, B, X) within the generic structure  $\text{ABX}_3$  or even minor changes in supposedly identical compositions<sup>[75,76]</sup> or concentrations<sup>[77]</sup> will render it difficult to compare and assess achievements unless the community moves toward reliable metrics that allow for comparability. We believe that radiative efficiencies, both PLQY and  $\text{EQE}_{EL}$ , are the most promising candidates for such metrics and would very much appreciate these numbers to be reported alongside

photovoltaic efficiencies.<sup>[2]</sup> In fact, other semiconductors such as kesterites<sup>[78–80]</sup> or III–V have similar bandgap tunability, entailing the same problem. In this regard, in a recent report, Green and Ho-Baillie<sup>[81]</sup> collected the highest reported radiative efficiencies for a broad number of photovoltaic systems, thereby highlighting the importance of the external radiative efficiency (PLQY) in limiting the  $V_{OC}$  and overall performance of such state-of-the-art devices.

In Figure 6c, the QFLS of four different HTL/perovskite films were compared to the QFLS of perovskite/(LIF)/ $\text{C}_{60}$  films, the corresponding p-i-n stacks, and the final device  $V_{OC}$ .<sup>[31]</sup> It was found that for efficient cells ( $>18\%$  PCE), the  $V_{OC}$  of the cells (columns) approaches the QFLS of the corresponding p-i-n stacks (black stars) within a small error ( $<20 \text{ meV}$ ). This was also confirmed for n-i-p-type cells based on  $\text{SnO}_2$  and  $\text{TiO}_2$ . The QFLS- $V_{OC}$  match implies that: (a) the dominant free energy losses occur at the perovskite/transport layer interfaces, (b) the *inferior* interface dominates the energy loss, and (c) completion of the device by the addition of contact metals does not introduce significant losses. It was further found that the perovskite top surface and its interface with *organic* CTLs—fullerenes for p-i-n devices and spiro-OMeTAD for n-i-p devices—appears to be the critical interface in the efficient devices. This may be an intrinsic property of interfaces involving organic semiconductors—in particular fullerenes<sup>[82]</sup>—but can potentially be overcome by addressing this very limiting interface properly, as we will discuss next.

The results were corroborated by drift-diffusion simulations which confirmed the QFLS- $V_{OC}$  match only in case of an energy alignment between the perovskite and the transport layers.<sup>[31]</sup> The simulations also highlighted the importance of energy level alignment between the perovskite and the CTLs, and suggest that a high built-in voltage of at least  $\approx 1.0 \text{ V}$  is required in order to reproduce the experimental current–density versus

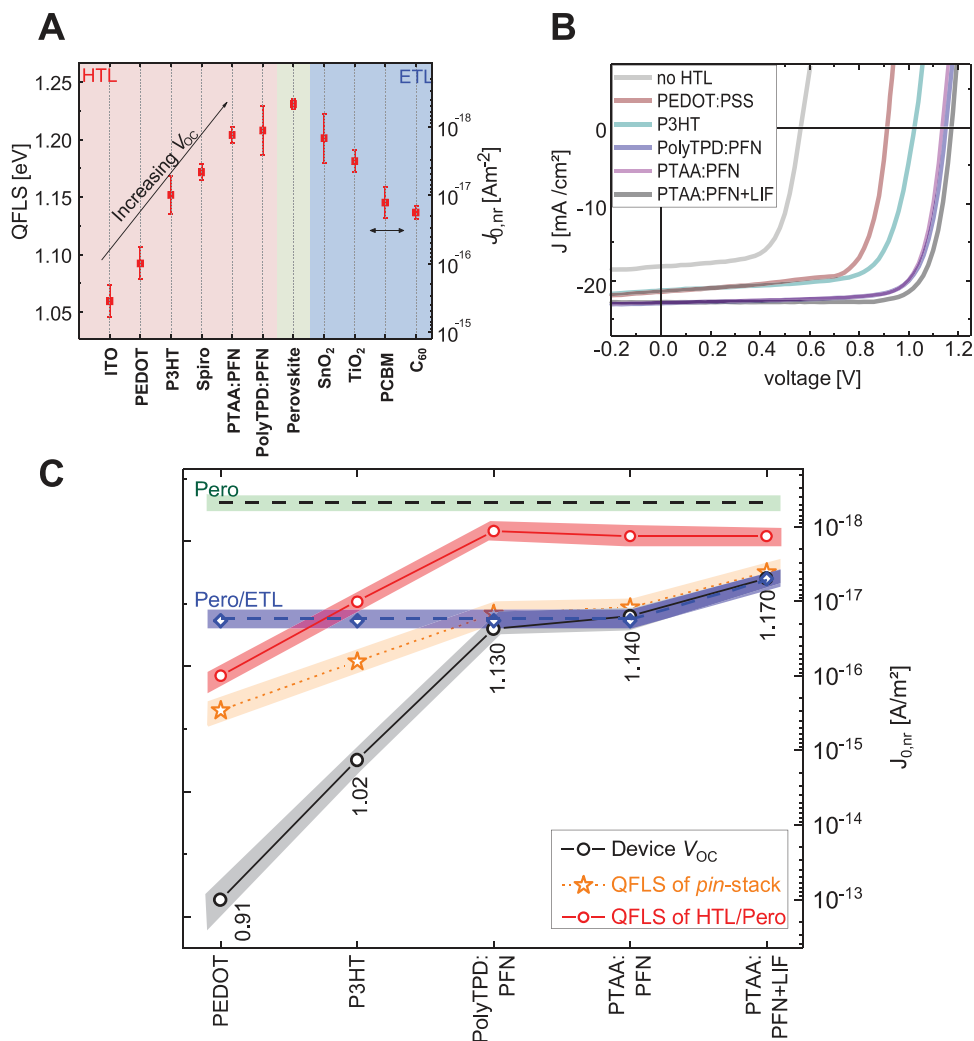


**Figure 6.** A) The quasi-Fermi level splitting as deduced from absolute photoluminescence measurements in the perovskite absorber without and various transport layers being present (hole CTLs are shown in red, electron CTL in blue). The corresponding thermal nonradiative recombination current ( $J_{0,nr} = J_0 - J_{0,rad}$ ) is plotted on the right. B) The current density versus voltage ( $J$ - $V$ ) characteristics of the p-i-n type cells with different conjugated polymers serving as a hole-transporting layer and with  $\text{C}_{60}$  as the ETL. In the “PTAA:PFN+LiF” device, a thin layer of LiF had been added between the perovskite and the  $\text{C}_{60}$  to reduce interfacial recombination. C) The average  $V_{OC}$  (black line) of cells shown in (B) as compared to the average QFLS of the corresponding HTL/perovskite and perovskite/ $\text{C}_{60}$  bilayers, as well as the QFLS of the p-i-n stacks, is shown in red, blue, and orange, respectively. The brown line represents the QFLS of the neat bulk material on fused silica, which also separates the interface (shaded purple area) and bulk limited regime (shaded orange area). A–C) Reproduced with permission.<sup>[31]</sup> Copyright 2019, Royal Society of Chemistry.

voltage ( $J$ - $V$ ) curves. However, in devices with energetically misaligned CTLs, a QFLS- $V_{OC}$  mismatch exists (Figure 6c) due to additional recombination losses at the interfaces or contacts. These energy offsets were further confirmed with ultraviolet photoelectron spectroscopy (UPS) and DC capacitance measurements.<sup>[31]</sup> Such internal voltage drops were earlier proposed by Wu et al.<sup>[65]</sup> who observed an identical PL yield of cells with different external  $V_{OC}$ s where  $\text{TiO}_2$  was annealed in different gas environments. This potentially impacted its work function and electron affinity and thereby the energy alignment with respect to the perovskite layer. Moreover, this may also rationalize the mismatch obtained by Guo et al.<sup>[83]</sup> when comparing  $V_{OC}$  in devices and QFLS calculated from rate constants, albeit the authors come in part to a different conclusion, namely, that in some cases bulk recombination is predominant, which

would be only possible if interfacial recombination is practically overcome in these cells.

### 3.1. Quantification of Recombination Currents at $V_{OC}$

In order to quantify the parallel recombination currents at  $V_{OC}$ , we consider that the PLQY is a measure of the ratio of emitted ( $\phi_{em}$ ) to absorbed photons ( $\phi_{abs}$ ), which equals—at  $V_{OC}$ —the radiative recombination current density divided by the total recombination current ( $J_{R,tot}$ ). The latter is a sum of radiative recombination and all nonradiative recombination losses in the bulk ( $J_{nr,B}$ ) and the interfaces ( $J_{nr,p/i}$  and  $J_{nr,i/n}$ ) and potentially other recombination currents at the metal contacts<sup>[31,84]</sup>

$$\text{PLQY} = \frac{\phi_{\text{em}}}{\phi_{\text{abs}}} = \frac{J_{\text{rad}}}{J_{\text{R,tot}}} = \frac{J_{\text{rad}}}{J_{\text{rad}} + J_{\text{non-rad}}} \quad (5)$$

$$= \frac{J_{\text{rad}}}{J_{\text{rad}} + J_{\text{nr,B}} + J_{\text{nr,p-i}} + J_{\text{nr,i-n}} + \dots}$$

Using the last expression of the PLQY allows writing the  $\mu$  (Equation (4)) as a function of all nonradiative recombination currents

$$\mu = k_{\text{B}}T \ln \left( \frac{J_{\text{rad}}}{J_{\text{rad}} + J_{\text{nr,B}} + J_{\text{nr,p-i}} + J_{\text{nr,i-n}} + \dots} \cdot \frac{J_{\text{G}}}{J_{0,\text{rad}}} \right) \quad (6)$$

Equation (6) highlights the impact of parallel recombination currents on the QFLS. The situation of the cell at  $V_{\text{OC}}$  is perhaps best compared to a bucket<sup>[85]</sup> with the water level representing the cells'  $V_{\text{OC}}$ . A constant water stream fills the bucket which corresponds to the generation current density from the sun.<sup>[30]</sup> The holes in the bucket represent the recombination losses at  $V_{\text{OC}}$  in the bulk, interfaces, etc. Depending on the exact size of the holes, the water level will change, and so will the  $V_{\text{OC}}$  of the device. The absolute PL approach allows estimating the recombination currents upon knowledge of the  $J_{\text{rad}}$  which is obtained from  $J_{0,\text{rad}}$  according to Equation (3). The latter can be quantified from the overlap of the cells' EQE and black body spectrum at 300°K.<sup>[86–88]</sup> Measurement of the PLQY of the different stack layers allows then quantification of the nonradiative recombination currents in the bulk and at the interfaces according to Equation (5). We note that the recombination currents need to be known at the QFLS of the final cell

which requires the knowledge of the ideality factor of the QFLS of the individual layers. The obtained recombination currents at  $V_{\text{OC}}$  for a standard p-i-n-type cell with PTAA:PFN as HTL and  $\text{C}_{60}$  as ETL are shown in Figure 7.

We want to emphasize that Figure 7a,b represents the recombination currents in the situation of an already well-performing perovskite cell. Should the defect density is much higher, recombination within the perovskite may dominate and even excellent contact layers could not improve the radiative efficiency (we note that worse perovskite systems have been shown in the Supporting Information of ref. [31]). To state this in the bucket frame, the biggest hole will dominate the losses. It is therefore imperative to identify the predominant loss channel and reduce this first. In this sense, we believe that some of the reported improvements with respect to open-circuit voltage—stated to stem from an improved bulk through additives or different (post-)processing—may be in fact improvements at the interfaces to the adjacent layers. As a side note, considering the (often) significant impact of interfacial recombination on the overall recombination current at  $V_{\text{OC}}$ , the ideality factor must be strongly influenced by interfacial recombination as well. Efficient p-i-n-type cells exhibit ideality factors of  $\approx 1.4$ – $1.5$ ,<sup>[12,28,31]</sup> which may be interpreted as the competition between radiative bulk and nonradiative SRH recombination as stated above. However, given the fact that  $n_{\text{ID}}$  stays constant over a broad range of intensities and that the nonradiative interfacial recombination is roughly  $\approx 15\times$  stronger at the perovskite/ $\text{C}_{60}$  interface compared to the radiative recombination in the bulk, it becomes apparent that some earlier interpretations of  $n_{\text{ID}}$  in terms of the dominant recombination pathway need to be revisited.

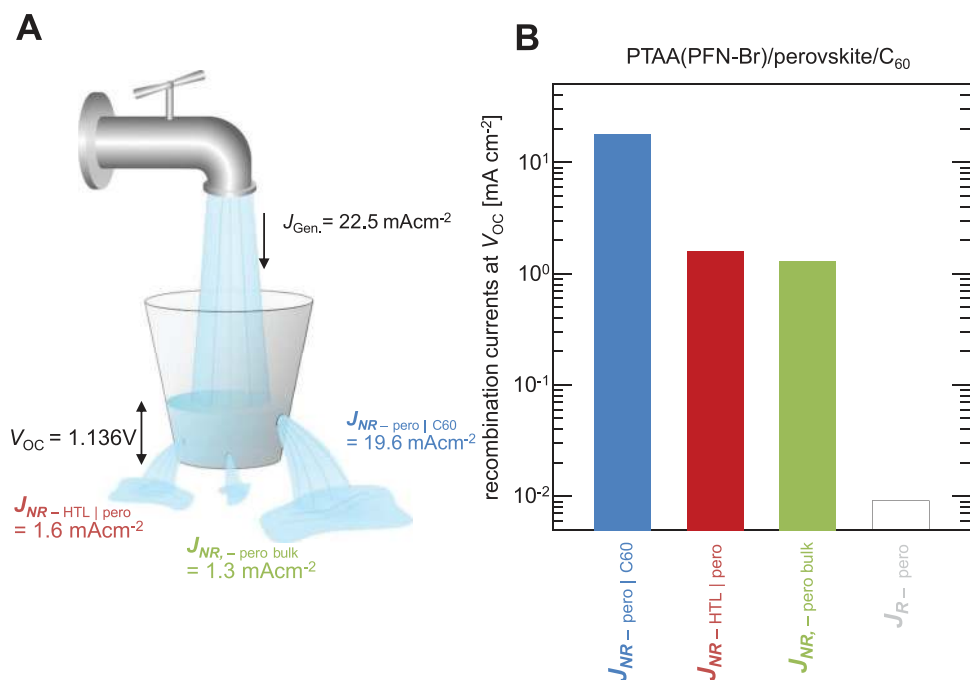


**Figure 7.** A) An ITO/PTAA/PFN-Br/perovskite/ $\text{C}_{60}$ /BCP/Cu solar cell under AM1.5G illumination at  $V_{\text{OC}}$ , illustrated by a bucket with holes. The holes in the bucket depict the recombination currents at  $V_{\text{OC}}$  (radiative bulk recombination is negligible and not shown). B) The recombination at the perovskite/ $\text{C}_{60}$  interface greatly outweighs the recombination in the perovskite bulk and at the HTL/perovskite interfaces. Adapted with permission.<sup>[31]</sup> Copyright 2019, Royal Society of Chemistry.

#### 4. Recombination Kinetics Revealed by Transient Measurements

While steady-state PL allows quantifying the recombination losses in the bulk, interfaces, and/or metal contacts, little is known how and at which rates recombination proceeds exactly at the interfaces. In particular, the steady-state PL measurements cannot disclose whether the addition of a transport layer worsens the performance because of an increased rate of recombination at the perovskite surface, across the perovskite/CTL interface, or by introducing recombination within the transport layers. In order to resolve the kinetics of bulk and interfacial recombination in perovskite films and solar cells, transient techniques with high time resolution are required. The most popular technique in the community is arguably TRPL.<sup>[28,89–91]</sup> Other transient techniques that have been applied less frequently to perovskite thin films include TRMC,<sup>[29]</sup> TAS,<sup>[92,93]</sup> or TRS,<sup>[20]</sup> and transient terahertz spectroscopy (THz, OOTP).<sup>[94]</sup> These techniques allow to track the fate of charges from below picoseconds to milliseconds, which provided deep insights into the fundamental recombination processes in the bulk and interfaces, however, the accurate implementation of these measurements is more challenging as well as a solid interpretation of the results. In contrast to the steady-state PL emission at  $V_{OC}$ , the TRPL decay is influenced by numerous processes. This is because the PL intensity is proportional to the product of the free electron and hole density on the perovskite layer (while TAS, TRMC, or THz yield a weighted sum of the two densities). It is, therefore, often difficult to disentangle the actual recombination loss in the TRPL signal from processes which depopulate only one of the two carrier reservoirs (electrons or holes). As such, the PL decay of a perovskite/CTL stack may be dominated by the transfer of charges to the transport layers, while the recombination of the remaining charges contribute only little to the transient.<sup>[10,90]</sup>

As pointed out above, PL is a sensitive measure of the product of electron and hole densities in the perovskite absorber. In case of a neat perovskite film, at sufficiently low fluences, a mono-exponential decay is usually observed, which has been assigned to a first-order loss process, for example, trapping and trap-assisted recombination, or radiative recombination with doping-induced background charges. If CTLs are attached to the perovskite an accelerated (sometimes multi-exponential) decay is observed, which has been explained by the extraction of majority charges,<sup>[95]</sup> fast interfacial recombination, or a combination of both. A comprehensive description of charge transfer and recombination processes at the perovskite/transport layer interfaces based on TRPL has been recently presented by Krogmeier et al.<sup>[96]</sup> who corroborated their experimental study on perovskite/PCBM bilayers with transient *drift-diffusion* simulations. The authors predicted that the TRPL decay at low fluences is determined by the rapid extraction of photogenerated electrons to the PCBM layer at early times while interfacial recombination dominates the decay at latter times, as shown in **Figure 8**. While these two regimes might be experimentally difficult to disentangle, application of the transient simulation allowed the authors to quantify the velocity of charge transfer and recombination at the perovskite interface. The authors concluded that the interfacial

transfer and recombination velocities could be readily obtained at low fluences ( $\approx 1 \text{ nJ cm}^{-2}$ ) although they noted that this condition might be difficult to realize experimentally. In contrast, at higher intensities, the obtained differential lifetime  $\tau_{PL}(t) = -\left(\frac{dn(\phi_{PL}(t))}{dt}\right)^{-1}$  can be substantially influenced by the accumulation of charges at the interfaces and the concurrent built-up of a space charge field, which would lead to erroneous (underestimated) lifetimes. For a perovskite/PCBM film, the authors quantified a charge transfer and recombination velocity to be  $S_T = 5300 \text{ cm s}^{-1}$  and  $S_R = 200 \text{ cm s}^{-1}$ , respectively. Nevertheless, there are multiple processes that could potentially lead to a multi-exponential TRPL decay, such as a graded generation profile or trap-filling and in many experimental studies only a single exponential decay is observed. Typical surface recombination velocities induced by the transport layers range from  $\approx 10$  to  $10^4 \text{ cm s}^{-1}$ , where—for the case of  $\text{CH}_3\text{NH}_3\text{PbI}_3$ —the former puts the potentially obtainable  $V_{OC}$  close to 1.3 V and the efficiency to  $>27\%$  if high current densities can be preserved ( $>23 \text{ mA cm}^{-2}$ ) and the FF would approach the radiative limit ( $\approx 90\%$ ).<sup>[30,97]</sup>

TRMC is an optical pump microwave-probe technique that measures the photoconductivity of charge carriers ( $\sigma$ ) from absorbed microwave power ( $\Delta P/P$ ) with a GHz frequency as a function of delay time ( $\Delta P/P = c\sigma$ ), where  $c$  is a cavity-dependent prefactor.<sup>[98]</sup> The photoconductivity is given by the mobility-weighted sum of the densities of free electron and hole density,  $n_e$  and  $n_h$ :  $\sigma = e\sum(n_e\mu_e + n_h\mu_h)$ , with  $\mu_e$  and  $\mu_h$  being the respective mobilities. Considering that right after photogeneration, the photogenerated charge carrier density is equal for electrons and holes, given by the number of absorbed photons, the sum of the charge carrier mobilities can be readily quantified at early times. Assuming further that the free carrier mobilities remain at their initial values, the decay of the photoconductivity allows obtaining quantitative information on the kinetics of bulk recombination, interfacial charge transfer, and interfacial recombination. For example, Hutter et al.<sup>[29]</sup> analyzed the TRMC decay dynamics of neat MAPI films on glass and MAPI/CTL junctions using a global kinetic model based on the continuity equations for electrons and holes. They proposed that CTL-assisted recombination is a multistep process where the majority charge is first transferred to the CTL, followed by recombination with the photogenerated minority carrier on the perovskite (see **Figure 9**). For common CTLs—such as PCBM and  $\text{C}_{60}$ —the rate of electron transfer,  $k_e$ , is more than one order of magnitude faster than the rate of subsequent interfacial capture of the hole by the electron on the CTL,  $k_h$  (see table in **Figure 9**), meaning that the rate-limiting process is the interfacial charge recombination. Importantly, both rates were reduced by approximately one order of magnitude when exchanging the  $\text{C}_{60}$  by higher-adduct fullerenes such as ICBA. ICBA has an  $\approx 0.2 \text{ eV}$  higher-lying lowest unoccupied molecular orbital (LUMO) than PCBM, which may explain the reduction in the electron transfer rate. The picture of fast electron-transfer to PCBM followed by slow interfacial hole recombination is also in line with findings from transient lateral conductivity studies by Leijtens et al.<sup>[17]</sup>

TAS (either in transmission or reflection mode) relies on the sensitive measurement of the photoinduced change in

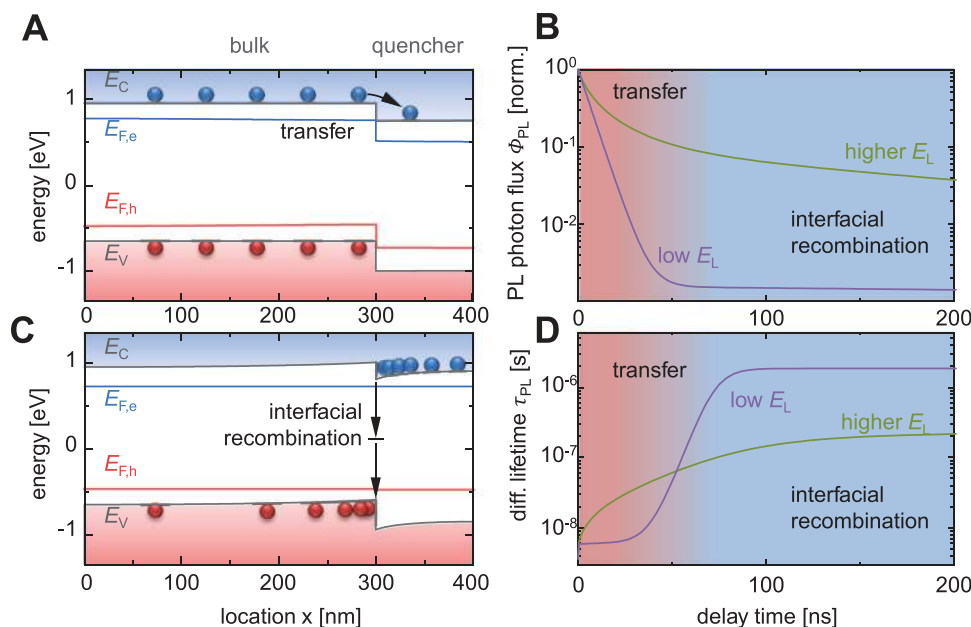


**Figure 8.** Results from 1D drift-diffusion simulations of TRPL on a perovskite/PCBM bilayer. A) Band diagram shortly after the laser pulse. Charge carriers are generated in the bulk and electrons transfer to the quencher. B) Band diagram for longer delay times. Charge carriers accumulate at the interface due to their mutual Coulomb attraction, leading to increased interfacial recombination. C) TRPL signal for two laser fluences ( $E_L$ ), both displaying two slopes, assigned to electron transfer and interfacial recombination. D) Differential lifetime showing two constant, clearly distinguishable regions for low laser fluences and a less distinguishable case for higher light intensities, where the latter case is affected by due to an accumulation of charge carriers. An interface recombination velocity of  $S_R = 10 \text{ cm s}^{-1}$  was assumed and  $E_L$  is  $1 \text{ nJ cm}^{-2}$  for the low fluence case and  $100 \text{ nJ cm}^{-2}$  for the high fluence case. A–D) Adapted with permission.<sup>[96]</sup> Copyright 2018, Royal Society of Chemistry.

absorption/reflection ( $\Delta\text{OD}$ ) as a function of the delay between a pump and a probe pulse. State-of-the-art laser equipment allows performing measurements with high sub-ps time-resolution. The absorption spectra comprise different features associated with ground-state bleaching (GSB), stimulated emission, and/or photoinduced absorption (PIA) of photogenerated charges, but may also comprise associated changes of the refractive index<sup>[99]</sup> and thus reflectivity of the stack according to the Kramers–Kronig relation.<sup>[99]</sup> Pioneering works using TAS on perovskite/CTL heterojunctions

suggested ultrafast injection ( $<200 \text{ fs}$ ) of photogenerated charges into PEDOT:PSS and PCBM,<sup>[93]</sup> and other transport layers,<sup>[92,100]</sup> much faster than the timescales of interfacial charge transfer and recombination as recorded by TRPL and TRMC as noted above. Considering that the absorption features of polarons on the CTLs are generally distinct from the photoinduced signals in the perovskite layer,<sup>[92,93]</sup> the transfer of charge can be readily visualized. **Figure 10** shows the PIA and GSB as measured on a perovskite film on glass, while the presence of a PEDOT:PSS underneath the perovskite

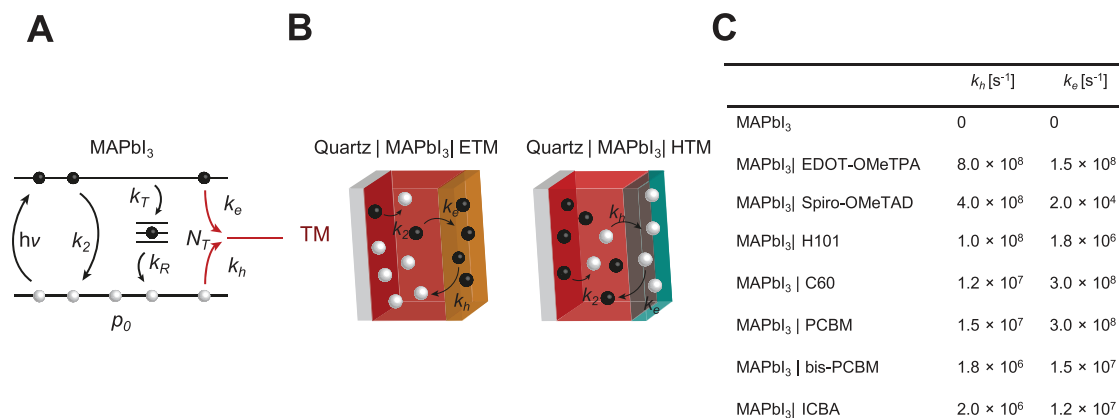


**Figure 9.** The kinetic model developed by Hutter et al.<sup>[29]</sup> for charge recombination across the interface between MAPbI<sub>3</sub> and an adjacent CTL. Interfacial recombination involves the extraction of a majority carrier (e.g.,  $k_h$  to the HTM) followed by its recombination with the remaining minority carrier in the perovskite (e.g.,  $k_e$  to the HTM). The table shows the obtained charge transfer and recombination rate constants in different bilayers. A–C) Adapted with permission.<sup>[29]</sup> Copyright 2017, Wiley-VCH.

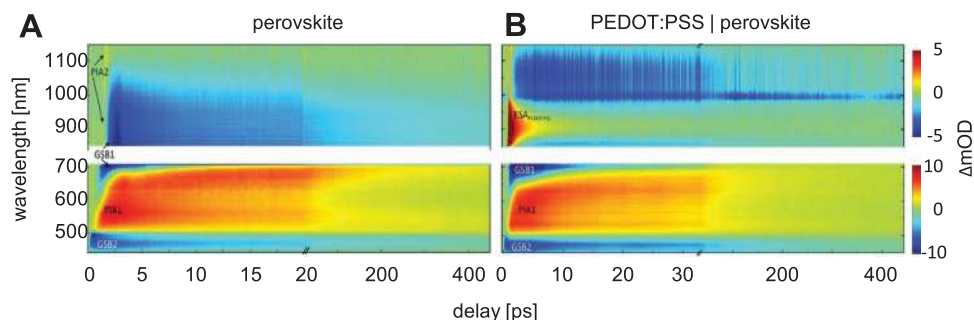


**Figure 10.** A,B) 2D color plots showing the change in absorption ( $\Delta m_{OD}$ ) across a large spectral range versus delay time measured on a neat perovskite ( $\text{CH}_3\text{NH}_3\text{PbI}_{3-x}\text{Cl}_x$ ) film and a perovskite/PEDOT:PSS bilayer. The TAS of the neat perovskite film shows fairly long-lived ground state bleaches at 480 nm (GSB2) and 775 nm (GSB1) and a photoinduced absorption signal at 600 nm (PIA1), in addition to a rapidly decaying transient absorption signal in the near-infrared (PIA2). In the sample with the PEDOT:PSS present, the immediate appearance (<200 fs) of the signal at 900 nm ( $\text{ESA}_{\text{PEDOT:PSS}}$ ) was assigned to holes being injected into PEDOT:PSS. We note that this signal decays rapidly with a time constant of 0.7 ps. A pump wavelength of 388 nm with a fluence of  $25 \mu\text{J cm}^{-2}$  was used. A,B) Adapted with permission.<sup>[93]</sup> Copyright 2018, Wiley.

layer demonstrated a sub-ps charge transfer of charges to the HTL layer. The impact of the high fluence ( $25 \mu\text{J cm}^{-2}$ , corresponding to carrier densities at  $\approx 1000$  suns) in these results needs to be carefully considered. Moreover, the decay of the polaron signal in the PEDOT:PSS containing film is remarkably fast (0.7 ps). This time constant is at least three orders of magnitude faster than typical interfacial recombination lifetimes on timescales above nanoseconds. This discrepancy suggests that transient measurements at high excitation conditions may be dominated by processes which are not visible under application-relevant conditions.

## 5. Suppression of Recombination

Having demonstrated the importance of interfacial recombination through steady-state and transient measurement techniques, the last part of this progress report aims at highlighting several selected, promising optimization strategies in order to suppress nonradiative recombination with particular focus on interfacial recombination. The general outline of the presented optimization strategies is as follows: (1) energy alignment, (2) suppression of nonradiative defect recombination at the interfaces and the perovskite surface, and (3) finally overcoming interfacial recombination.

### 5.1. Energy Level Alignment

One of the most debated topics in the community is the importance of energy level alignment between the perovskite and the transport layers. Although the topic is far from being fully understood, from a theoretical point of view, it is expected that having aligned perovskite/CTL energy levels is highly beneficial to maximize the  $V_{OC}$  of the cells. The reason is that in order to yield the maximum achievable  $V_{OC}$  the electron and hole quasi-Fermi levels within the illuminated perovskite absorber layer need to perfectly align with the Fermi levels of the respective contacts. In other words, the electron (hole) quasi-Fermi levels must not exhibit any tilt within the perovskite semiconductor or with the electron (hole) transporting layers. Ideally, this case

is realized if the electron (hole) current density is zero at any point in the device, meaning that recombination at internal interfaces or at the electrodes is negligible compared to bulk recombination in the perovskite layer.<sup>[32,101]</sup> Now, any energy level offset would exponentially increase the charge carrier density within the CTL, causing an exponential increase of the interfacial recombination current and concurrently introducing a bending of the quasi-Fermi levels of the majority charge carrier.<sup>[31,65]</sup> These basic considerations are readily confirmed from drift-diffusion simulations on n-i-p and p-i-n-type perovskite solar cells as shown in Figure 11a,b.<sup>[65]</sup> An energy level offset of 0.3 eV between the perovskite and the  $\text{C}_{60}$  thereby leads to a similar voltage loss due to the downward bending of the electron quasi-Fermi level. Indeed, as a rule of thumb, we find that any majority carrier band offset leads to an equal loss in  $V_{OC}$  in case the interface with the offset is determining the recombination loss.<sup>[31]</sup>

From an experimental perspective, it has been shown that the energetic offset at the interface between the perovskite and the hole or electron transport layer has a large influence on the device  $V_{OC}$  (e.g., Schulz et al.,<sup>[102]</sup> Polander et al.,<sup>[103]</sup> us,<sup>[28]</sup> and others<sup>[104–106]</sup>). Figure 11b,c shows the case where MAPI was combined with different fullerene derivatives in a p-i-n-type architecture. Employing  $\text{C}_{60}$  led to a poor  $V_{OC}$  of only 1.03 V, indicating an unfavorable energy alignment. Indeed, inverse photoelectron spectroscopy (IPES) showed that the LUMO level of  $\text{C}_{60}$  lies below the conduction band minimum (CBM) of the MAPI, causing accumulation of electrons on the ETL. The energetic situation changes drastically when replacing  $\text{C}_{60}$  with the higher adduct fullerenes, where the LUMO now lies 0.6 eV above the CBM in case of ICTA. This inversion of the energy offset at the hybrid interface goes along with a significant improvement of the  $V_{OC}$ . These spectra also display a significant density of states below the specified LUMO position which may enable the efficient extraction of electrons even in case of PCBM, ICBA, or ICTA. However, in contrast to the expectation from the interface energetics, the highest  $V_{OC}$  was realized by inserting an ultrathin polystyrene (PS) interlayer between MAPI and  $\text{C}_{60}$ . The reasons for this will be discussed next. More recently, higher adduct fullerenes have been used as ETLs in low bandgap mixed Pb–Sn-based perovskite solar

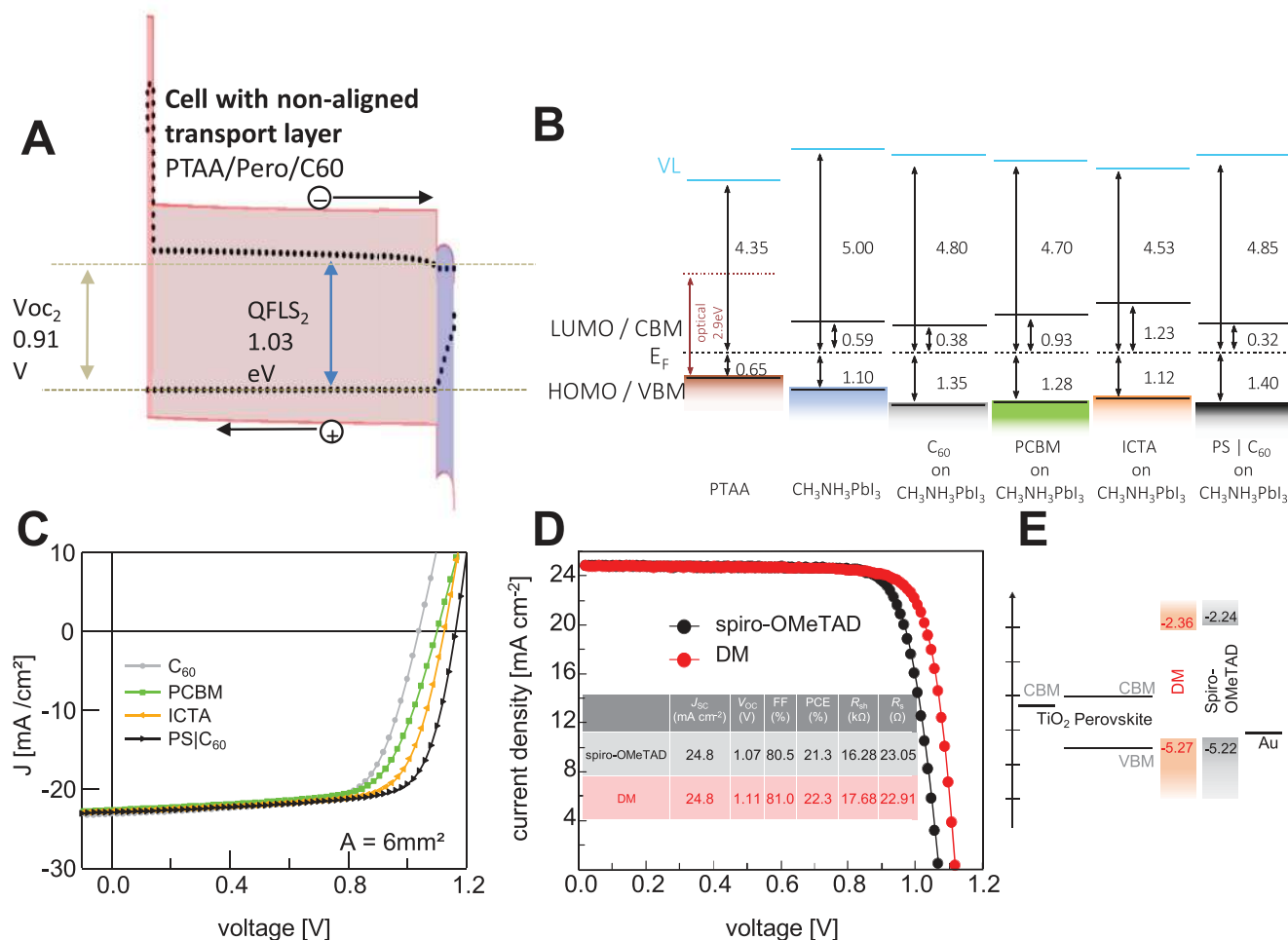


**Figure 11.** A) Device simulations of perovskite cells (ITO/PTAA/perovskite/C<sub>60</sub>/BCP/Cu) with and without an energy offset of 0.3 eV at the perovskite/C<sub>60</sub> interface which leads to considerable  $V_{OC}$  loss of 0.27 V (from 1.18 to 0.91 V) due to a built-up of charge carriers at the electron selective contact, which increases the interfacial recombination. B) Energy levels of MAPI and of different ETLs on top of the perovskite (C<sub>60</sub>, PCBM, ICTA, and PS/C<sub>60</sub>) as obtained from ultraviolet photoelectron spectroscopy (UPS) and inverse photoelectron spectroscopy (IPES). A (detrimental) downhill energy level offset was obtained between the perovskite and the C<sub>60</sub> layer, while PCBM and ICTA show an uphill energy level offset. C) The  $J$ - $V$  curves of the corresponding p-i-n devices demonstrating the improved  $V_{OC}$  from C<sub>60</sub> to PCBM to ICTA to PS/C<sub>60</sub>. D)  $J$ - $V$  characteristics of n-i-p devices with the hole-transporting layer formed either by the traditional spiro-OMeTAD or from the fluorene-terminated spiro-based molecule DM. Devices with DM exhibit a significantly larger  $V_{OC}$ , resulting in record efficiencies of above 22%. E) The improvement was assigned to the better-aligned ionization potential of DM with respect to the perovskite valence band. A) Adapted with permission.<sup>[31]</sup> Copyright 2019, Royal Society of Chemistry. B,C) Adapted with permission.<sup>[28]</sup> Copyright 2017, Wiley-VCH. C,D) Adapted with permission.<sup>[108]</sup> Copyright 2018, Springer Nature.

cells, reaching an impressive  $V_{OC}$  of 0.89 V (at a radiative limit of 0.97 V).<sup>[107]</sup> This was attributed to a better energy alignment and reduced nonradiative losses. Finally, we note that one of the major recent efficiency advancements of n-i-p perovskite solar cells was achieved by introducing a novel, fluorine-terminated hole transport material (which the authors called “DM”), with a higher ionization potential (IP) compared to the prototypical spiro-OMeTAD. The improved  $V_{OC}$  was attributed to the better alignment of the IP of the HTM and the valence band of the perovskite. This enabled a steady-state power conversion efficiency of 22.85% for small-area cells and a certified PCE of 20.9% of a 1 cm<sup>2</sup> device (Figure 10d,e).<sup>[108]</sup>

Despite these successes, several other experimental studies showed little to no correlation between the energy levels of the transport layers and the device  $V_{OC}$ .<sup>[109–111]</sup> For example, Belisle

et al. studied the correlation between the  $V_{OC}$  and the IP of several hole transport layers in p-i-n cells. Despite the significant increase of the IP from 5.1 to 5.35 eV, the  $V_{OC}$  remained at around 1 V (with one exception). This indicates that more research is necessary to understand the role of energy level alignment. We also note that the determination of the energy level alignment is an experimentally difficult task and the energetic at the hidden perovskite/CTL interface in the complete stack is generally not accessible by UPS and IPES. Recent experimental work also highlighted the role of band dispersion on the UPS spectra of polycrystalline perovskite samples.<sup>[112]</sup> Finally, the IP, electron affinity (EA), and work function of the perovskite have been shown to depend sensitively on the level of exposure to oxygen, water, and even light; this also includes the magnitude of surface band bending within the perovskites,



induced by gap (defect) states.<sup>[60]</sup> The key consideration in this regard is that the energy levels of the layers need to be measured in the actual cell stacks, as values of IP, EA, and work function determined for each individual material do not allow accurate estimation of the interfacial energy level alignment based on the Schottky–Mott limit. For example, several possible interfacial phenomena lead to a charge rearrangement—and therefore to modified energy levels—upon contact of two materials, ranging from the “push-back” effect in the physisorption regime, to Fermi level pinning at valence and conduction band edges, covalent interactions with polar character, or band bending due to surface states.<sup>[113,114]</sup> In this regard, it is interesting to note that cross-sectional Kelvin probe measurements have been performed to quantify the local contact potential difference (LCPD, i.e., the difference in surface potential) across the whole cross section of the devices, which was polished using a focused ion beam.<sup>[115,116]</sup> If the sample is in the dark at SC, the Fermi level is flat, meaning that under these conditions, KP measures the local work function along the sample cross section. Illuminating the sample and/or increasing the bias causes a redistribution of charge (ions, electrons, and holes) which becomes visible through changes in the local KP potential. The authors observed remarkably different LCPD distribution under short- and open-circuit conditions in cells with TiO<sub>2</sub> and C<sub>60</sub> as ETLs. However, the question remains how the surface energetics (as created with the ion beam) compares to bulk properties of the film. Nevertheless, samples which are prepared in the same way can be compared which has provided useful insights that are difficult to assess otherwise.

### 5.2. Interfacial Optimizations: Interlayers, Graded Junctions, and Doping

Other optimization strategies were often targeted at passivating traps at the perovskite surface<sup>[22,23,117,118]</sup> or grain boundaries, or through the insertion of high bandgap interlayers between the perovskite and the CTL.<sup>[11,19,28,119,120]</sup> Examples of successfully applied interlayers to improve the  $V_{OC}$  include PS,<sup>[28,119]</sup> Ga<sub>2</sub>O<sub>3</sub>,<sup>[120]</sup> choline chloride,<sup>[19]</sup> LiF,<sup>[11]</sup> and poly(methyl methacrylate) (PMMA),<sup>[118,121]</sup> or most recently phenethylammonium iodide (PEAI).<sup>[122]</sup> While qualitative explanations were suggested to explain the observed performance improvements, little is known how these interlayers work on a fundamental level. For example, a wide-gap interlayer may passivate defects, slow down the extraction of the majority carriers, or suppress the transfer of the minority carrier to the CTL, thereby suppressing recombination. In an ideal scenario, such strategies passivate surface traps and suppress the across-interface recombination by blocking the minority carriers from the interface while still allowing the majority carriers to efficiently tunnel through the barrier.<sup>[119]</sup> However, the addition of interlayers often comes at the price of charge extraction losses due to the series resistance of the interlayer. Another possibility to suppress recombination which is inspired by silicon solar cells, although much less exploited in the perovskite field, is to chemically dope the CTL or the perovskite in order to create a backfield which expels the minority carriers from the critical interface. For example, we have shown that adding SrI<sub>2</sub> into the perovskite precursor solution resulted in an

n-doped perovskite surface which led to a substantial improvement of the open-circuit voltage to 1.18 V in mixed quadruple cation perovskite cells (Figure 12d–f).<sup>[72]</sup> The  $V_{OC}$  could be further raised to 1.23 V by inserting an ultrathin layer of PS, however, at the price of FF losses as often the case with (wide-gap) interfacial layers. An attractive alternative approach is to engineer the perovskite bandgap at the interface to the CTL. For example, reduced recombination was attained by spin-coating a formamidinium bromide (FABr) precursor on an as-prepared mixed Br-poor perovskite, thereby forming a graded composition perovskite with a Br-enriched layer at the top surface. It was proposed that this higher bandgap top layer suppresses the transfer of electrons to the HTM, with the result of a substantial increase of the  $V_{OC}$  from 1.1 to 1.16 V.<sup>[123]</sup> More recently, Luo et al.<sup>[24]</sup> employed a similar secondary growth technique to create a perovskite surface layer with a wider bandgap and a more n-type character. Optimized devices p-i-n-type cells had a  $V_{OC}$  of 1.21 V, only 0.41 V lower than the bandgap of 1.62 V (Figure 12a–c).

### 5.3. Overcoming Interfacial Recombination

Although more complicated perovskite compositions including multiple cations and/or halides are becoming more and more popular across the community, the standard MAPI perovskite remains subject of substantial research, particularly for (co-) evaporated solar cells.<sup>[124]</sup> Today, record MAPI cells have allowed efficiencies above 21% PCE.<sup>[125]</sup> Moreover, as discussed above, MAPI exhibits a large QFLS close to the thermodynamic efficiency limit if the top surface is properly passivated as shown in Figure 1.<sup>[22]</sup> In this regard, Liu et al.<sup>[71]</sup> could recently add an extraordinary result. A special MAPI recipe based on lead acetate enabled perovskite cells with record open-circuit voltages of 1.26 V (with a bandgap of 1.6 eV) after light soaking for 10 min. The  $J$ – $V$  scans of the corresponding solar cells are shown in Figure 13a. Notably, an external PLQY of ≈8% was demonstrated in the full p-i-n stack (PTAA/MAPI/PCBM) and the final device, leaving the devices with only 60 mV loss in  $V_{OC}$  compared to the radiative limit. This result stands out not only because of its extraordinary low voltage loss but also because such performance was realized by optimizing the preparation scheme for the active absorber and the PCBM transport layer, leaving the chemical composition of the constituents unaffected. PCBM is generally considered to induce significant nonradiative losses (see above). For example, our comparison of MAPI devices with different fullerene-based ETLs<sup>[28]</sup> suggested that the inferior  $V_{OC}$  of PCBM-containing cells is intrinsic to the system and related to its fairly high electron affinity (and possibly too low ionization potential). The very high  $V_{OC}$  in the work by Liu et al., where the PCBM was coated directly onto an as-prepared perovskite, questions this simple picture and asks for a detailed analysis of the chemical and energetic structure at the interface. For example, Huang and co-workers<sup>[126]</sup> showed that postdeposition solvent annealing of the electron transport layer (PCBM) caused a significant increase in the  $V_{OC}$ . By combining results from X-ray and IS, the authors proposed that solvent annealing improves the structural order in the fullerene-based ETL, thereby reducing the energetic disorder and the density of low energy states in the ETL. In an

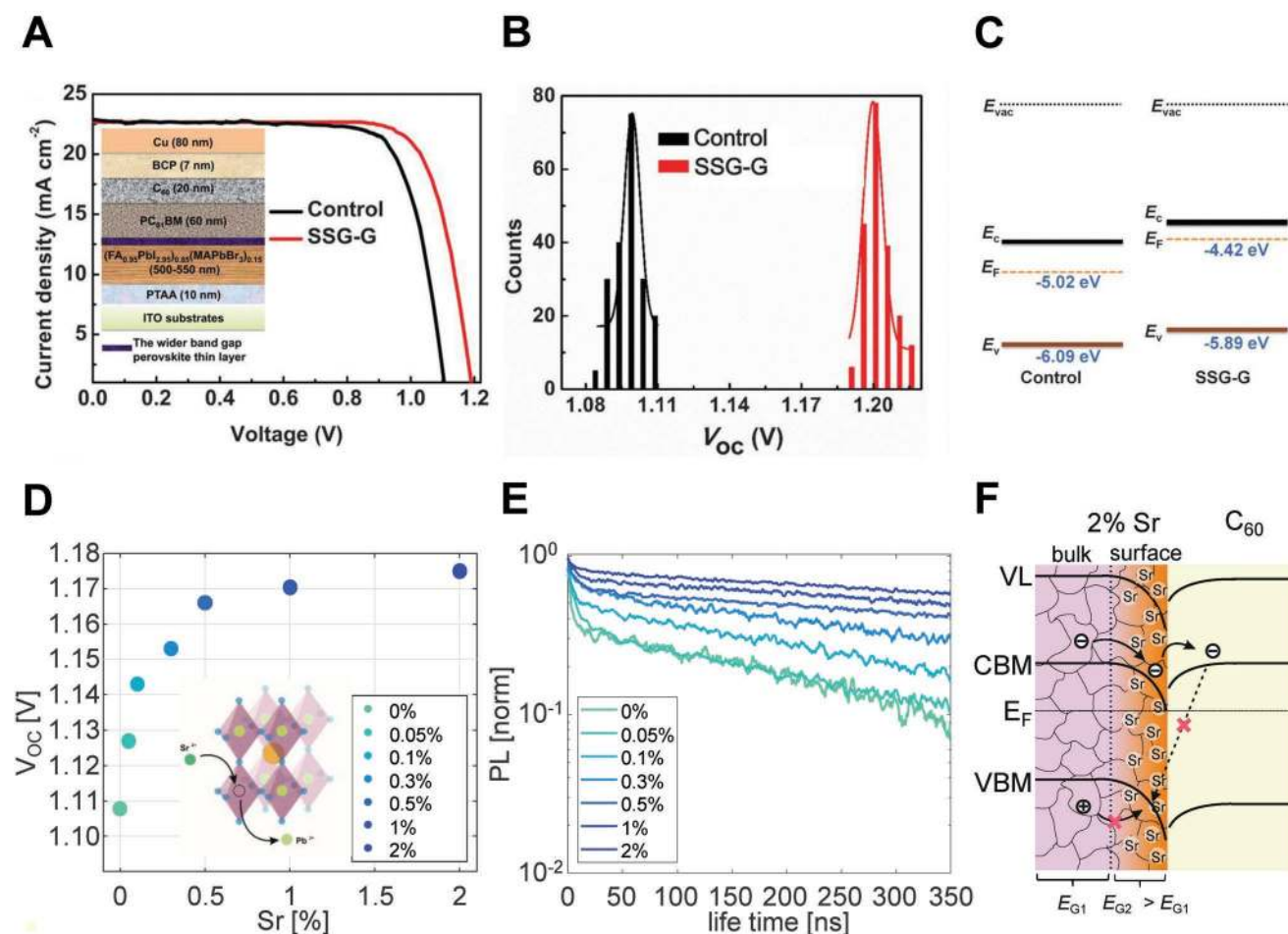


**Figure 12.** A–C)  $J$ – $V$  characteristics of p–i–n solar cells fabricated based on a “secondary perovskite growth approach (SSG-G)” which creates a perovskite surface with a larger bandgap and a more  $n$ -type character, both resulting in large  $V_{OC}$  gains (B). D–F) Addition of  $SrI_2$  into the precursor solution led to a significant increase in  $V_{OC}$  (D) and TRPL lifetime (E) of quadruple cation perovskite cells. F) Energy levels as obtained from UPS measurements which demonstrated the formation of a back-surface field which reduces interfacial recombination by repelling photogenerated minority carriers from the interface. A–C) Adapted with permission.<sup>[24]</sup> Copyright 2018, AAAS. D–F) Adapted with permission.<sup>[72]</sup> Copyright 2019, the Royal Society of Chemistry.

alternative approach, Jiang et al.<sup>[122]</sup> reduced losses at the perovskite/Spiro-OMeTAD interface in n-i-p cells by overcoating the perovskite with a thin layer of PEAI before adding the HTL on top. It was proposed that this procedure passivates the perovskite and thereby reduces nonradiative recombination at the top surface. Consequently, they realized an  $EQE_{EL}$  of 7% (at  $24 \text{ mA cm}^{-2}$  injection, shown in Figure 13d), corresponding to a voltage deficit of only  $\approx 70 \text{ mV}$ .<sup>[122]</sup> Other examples include secondary phases at the top and/or bottom surface,<sup>[24,72,123]</sup> polymeric,<sup>[28,118,119]</sup> salt,<sup>[23,127,128]</sup> or molecular<sup>[73,129]</sup> passivation. These are only a few demonstrations where interfacial recombination was significantly reduced.

Overall, we conclude that the  $V_{OC}$  will be primarily limited by: (1) unfavorable energy alignment, which can cause large  $V_{OC}$  losses through a mismatch between the internal QFLS and the external  $V_{OC}$ ; (2) defect recombination at the interfaces or (3) in the perovskite; or (4) by a low probability of photons to leave the cell. This is because the externally measurable luminescence efficiency and in turn the open-circuit voltage is reduced through a reduced emission probability. We

consequently expect four main strategies that will allow further improvements: (1) proper energy level matching between the perovskite and the transport layers; (2) reduction of interfacial recombination via efficient contact layer passivation; (3) optimization of the perovskite layer, for example, with secondary interfacial phases that passivate the bulk and the surfaces; and finally (4) optical management strategies facilitating light trapping and enhancing light outcoupling. We predict, that in the near future, optical management<sup>[130–132]</sup> will play a significant role and could push external PLQYs in full devices to values of GaAs solar cells (22.5%) and beyond.<sup>[133]</sup> Exemplary, by optimizing the light outcoupling<sup>[131,134–136]</sup> and reducing non-radiative recombination, red-emitting perovskite LEDs—with transport layers feasible for solar cells—have now surpassed 20% emission efficiency at low injection levels comparable to 1 sun illumination ( $J_{inj} = 18 \text{ mA cm}^{-2}$ , Figure 13e).<sup>[137]</sup> We believe that solar cells with even higher external luminescent efficiencies—and therefore  $V_{OC}$  and PCE—are well within reach. Although the exact mechanism behind the high  $V_{OC}$ 's in these devices remains to be fully understood and transferred into

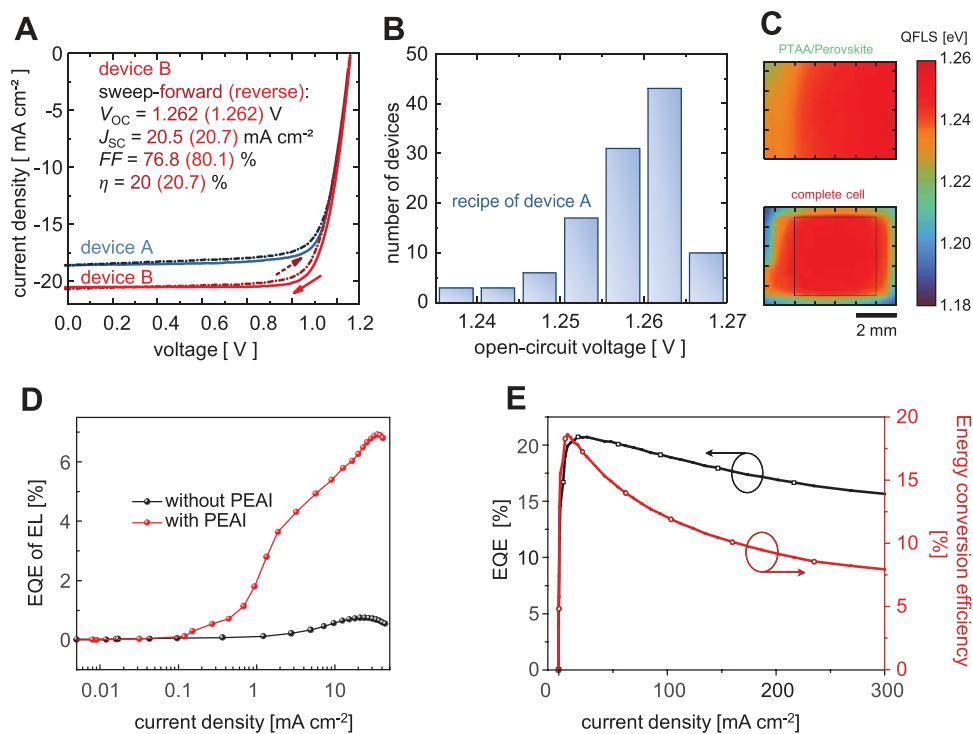


**Figure 13.** A,B) Liu et al.<sup>[71]</sup> recently showed very high open-circuit voltages of 1.26 V for methylammonium lead iodide perovskite cells. C) The PL quantum efficiency (PLQY) of the complete solar cell was quantified to be 8%, which was equal to the PLQY of the perovskite absorber layer, thus enabling a quasi-Fermi level splitting of 1.26 eV in the cells. D) n-i-p structured perovskite solar cell passivated with PEAI that exhibits an EQE<sub>EL</sub> of 6% at 20 mA cm<sup>-2</sup>. E) Perovskite LED based on micrometer-structured perovskite layers with LED efficiencies up to 20.7%. A–C) Adapted with permission.<sup>[71]</sup> Copyright 2018, American Chemical Society. D) Adapted with permission.<sup>[122]</sup> Copyright 2018, Springer Nature. E) Adapted with permission.<sup>[137]</sup> Copyright 2019, Springer Nature.

highly stable devices, it underlines the great potential of perovskite solar cells when essentially overcoming interfacial/surface recombination.

## 6. Conclusions

After ten years of research, the perovskite solar cell community has experienced incredible efficiency improvements from 3.9 to >25% in single-junction cells and 28% in tandem solar cells with a Si bottom cell. Alongside this rapid improvement, the community has reached a considerable understanding of the photophysical properties of the perovskite and the device operation. This progress report demonstrates recent advances in pinpointing the origin of nonradiative recombination losses in the perovskite bulk, the perovskite/CTL interfaces, and/or metal contacts through measurement of the absolute PL emitted from perovskite films with and without transport layers. These measurements reveal that the perovskite bulk would allow a QFLS that is very close to the thermodynamic limits and demonstrate that nonradiative recombination at the perovskite/CTL interfaces can consistently explain the open-circuit voltage losses of perovskite cells in n-i-p and p-i-n configurations for various transport layers. Intriguingly, improving the perovskite bulk will not result in further efficiency improvements if the interfaces do not improve concurrently. In fact, both interfaces need to be simultaneously optimized, though it has also been shown

that the majority of recombination losses in highly efficient devices happen at the top surface/interface (i.e., perovskite/fullerene or perovskite/spiro-OMeTAD in case of p-i-n of n-i-p devices, respectively). The quality of each interface in the perovskite solar cell stack can be readily checked by comparing the QFLS of perovskite films with and without the transport layers. Measurements on several efficient solar cells in p-i-n and n-i-p configuration further reveal a match between the internal and the external QFLS (i.e., the  $V_{OC}$ ) which indicates an alignment between the energy levels of the perovskite absorber and the CTLs. However, in less efficient cells with PEDOT:PSS and P3HT HTLs at the bottom, the QFLS can be larger than the  $V_{OC}$  due to energy level offsets across the interfaces. Although the absolute QFLS-PL approach allows quantifying the recombination currents in the bulk, interfaces, or metal contacts, the precise recombination pathway at the interfaces remains poorly understood today. Sophisticated all-optical transient and electrooptical measurement techniques such as TRPL, TRMC, THz, and TAS have enabled the community insights into the ultrafast processes of charge recombination within the perovskite bulk and interfaces as well as charge transfer to the transport layers. This allowed quantification of transfer and recombination rate constants which can consistently describe the  $V_{OC}$  of the final cells. Although much less employed today, TAS allows to assess even faster timescales and suggest ultrafast charge transport (<1 ps) into standard CTL such as PEDOT:PSS or PCBM which would be invisible to transient PL measurements

that are based on the concept of time-correlated single-photon counting. However, further research is required to cross-check results obtained from different transient methodologies. Finally, among the most debated topics in the field remain the impact of energy level alignment at the interfaces and its impact on cell performance. Although aligned perovskite/CTL energy levels are expected to be highly beneficial from basic considerations of charge accumulation and interfacial recombination, experimental evidence does not fully support these conclusions, which we believe is related to difficulties in assessing the true energy levels in the operational solar cells. Going forward, multiple promising optimization strategies have been recently proposed to further suppress nonradiative recombination. As such, it was recently demonstrated how to overcome interfacial recombination in MAPI and MAFAPbI<sub>3</sub> based perovskite cells. In the coming years, an improved understanding of the mechanisms that enable suppressed interfacial recombination will allow designing passivation strategies and new transport layers ideally suited for perovskite solar cells. Combining these strategies with elaborate light management will pave the way to surpass the efficiencies of monocrystalline silicon cells in the near future.

## Acknowledgements

The authors thank HyPerCells, a joint graduate school of the University of Potsdam and the Helmholtz-Zentrum Berlin, for support and T. Kirchartz, T. Unold and S. Albrecht for fruitful discussions.

## Conflict of Interest

The authors declare no conflict of interest.

## Keywords

interfacial recombination, open-circuit voltage, perovskite solar cells, photoluminescence

Received: April 30, 2019

Revised: August 19, 2019

Published online:

- [1] NREL, "Best Research-Cell Efficiencies", <https://www.nrel.gov/pv/assets/pdfs/best-research-cell-efficiencies.20190703.pdf> (accessed: August 2019).
- [2] M. A. Green, Y. Hishikawa, E. D. Dunlop, D. H. Levi, J. Hohl-Ebinger, M. Yoshita, A. W. Y. Ho-Baillie, *Prog. Photovoltaics* **2019**, *27*, 3.
- [3] K. Yamamoto, K. Yoshikawa, H. Uzu, D. Adachi, *Jpn. J. Appl. Phys.* **2018**, *57*, 08RB20.
- [4] K. Yoshikawa, H. Kawasaki, W. Yoshida, T. Irie, K. Konishi, K. Nakano, T. Uto, D. Adachi, M. Kanematsu, H. Uzu, K. Yamamoto, *Nat. Energy* **2017**, *2*.
- [5] K. A. Bush, A. F. Palmstrom, Z. (Jason) Yu, M. Boccard, R. Cheacharoen, J. P. Mailoa, D. P. McMeekin, R. L. Z. Hoye, C. D. Bailie, T. Leijtens, I. M. Peters, M. C. Minichetti, N. Rolston, R. Prasanna, S. Sofia, D. Harwood, W. Ma, F. Moghadam, H. J. Snaith, T. Buonassisi, Z. C. Holman, S. F. Bent, M. D. McGehee, *Nat. Energy* **2017**, *2*, 17009.
- [6] S. Albrecht, M. Saliba, J. P. Correa Baena, F. Lang, L. Kegelmann, M. Mews, L. Steier, A. Abate, J. Rappich, L. Korte, R. Schlattmann, M. K. Nazeeruddin, A. Hagfeldt, M. Grätzel, B. Rech, *Energy Environ. Sci.* **2016**, *9*, 81.
- [7] F. Sahli, J. Werner, B. A. Kamino, M. Bräuninger, R. Monnard, B. Paviet-Salomon, L. Barraud, L. Ding, J. J. Diaz Leon, D. Sacchetto, G. Cattaneo, M. Despeisse, M. Boccard, S. Nicolay, Q. Jeangros, B. Niesen, C. Ballif, *Nat. Mater.* **2018**, *17*, 820.
- [8] Oxford PV, "Oxford PV sets world record for perovskite solar cell", <https://www.oxfordpv.com/news/oxford-pv-sets-world-record-perovskite-solar-cell> (accessed: August 2019).
- [9] M. H. Futscher, B. Ehrler, *ACS Energy Lett.* **2017**, *2*, 2089.
- [10] W. Tress, *Adv. Energy Mater.* **2017**, *7*, 1602358.
- [11] M. Stolterfoht, C. M. Wolff, J. A. Márquez, S. Zhang, C. J. Hages, D. Rothhardt, S. Albrecht, P. L. Burn, P. Meredith, T. Unold, D. Neher, *Nat. Energy* **2018**, *3*, 847.
- [12] M. Stolterfoht, C. M. Wolff, Y. Amir, A. Paulke, L. Pedrigón-Toro, P. Caprioglio, D. Neher, *Energy Environ. Sci.* **2017**, *10*, 1530.
- [13] W. Tress, M. Yavari, K. Domanski, P. Yadav, B. Niesen, J. P. Correa Baena, A. Hagfeldt, M. Grätzel, *Energy Environ. Sci.* **2018**, *11*, 151.
- [14] W. S. Yang, B. Park, E. H. Jung, N. J. Jeon, Y. C. Kim, D. U. Lee, S. S. Shin, J. Seo, E. K. Kim, J. H. Noh, S. I. Seok, *Science* **2017**, *356*, 1376.
- [15] D. Bi, C. Yi, J. Luo, J.-D. Décoppet, F. Zhang, S. M. Zakeeruddin, X. Li, A. Hagfeldt, M. Grätzel, *Nat. Energy* **2016**, *1*, 16142.
- [16] T. S. Sherkar, C. Momblona, L. Gil-Escrig, J. Ávila, M. Sessolo, H. J. Bolink, L. J. A. Koster, *ACS Energy Lett.* **2017**, *2*, 1214.
- [17] T. Leijtens, G. E. Eperon, A. J. Barker, G. Grancini, W. Zhang, J. M. Ball, A. R. S. Kandada, H. J. Snaith, A. Petrozza, *Energy Environ. Sci.* **2016**, *9*, 3472.
- [18] L. M. Herz, *Annu. Rev. Phys. Chem.* **2016**, *67*, 65.
- [19] X. Zheng, B. Chen, J. Dai, Y. Fang, Y. Bai, Y. Lin, H. Wei, X. C. C. Zeng, J. Huang, *Nat. Energy* **2017**, *2*, 17102.
- [20] Y. Yang, M. Yang, D. T. Moore, Y. Yan, E. M. Miller, K. Zhu, M. C. Beard, *Nat. Energy* **2017**, *2*, 16207.
- [21] Y. Yang, Y. Yan, M. Yang, S. Choi, K. Zhu, J. M. Luther, M. C. Beard, *Nat. Commun.* **2015**, *6*, 7961.
- [22] I. L. Braly, D. W. DeQuilettes, L. M. Pazos-Outón, S. Burke, M. E. Ziffer, D. S. Ginger, H. W. Hillhouse, *Nat. Photonics* **2018**, *12*, 355.
- [23] M. Abdi-Jalebi, Z. Andaji-Garmaroudi, S. Cacovich, C. Stavrakas, B. Philippe, J. M. Richter, M. Alsari, E. P. Booker, E. M. Hutter, A. J. Pearson, S. Lilliu, T. J. Savenije, H. Rensmo, G. Divitini, C. Ducati, R. H. Friend, S. D. Stranks, *Nature* **2018**, *555*, 497.
- [24] D. Luo, W. Yang, Z. Wang, A. Sadhanala, Q. Hu, R. Su, R. Shivanna, G. F. Trindade, J. F. Watts, Z. Xu, T. Liu, K. Chen, F. Ye, P. Wu, L. Zhao, J. Wu, Y. Tu, Y. Zhang, X. Yang, W. Zhang, R. H. Friend, Q. Gong, H. J. Snaith, R. Zhu, *Science* **2018**, *360*, 1442.
- [25] M. Saliba, T. Matsui, K. Domanski, J.-Y. Seo, A. Ummadisingu, S. M. Zakeeruddin, J.-P. Correa-Baena, W. R. Tress, A. Abate, A. Hagfeldt, M. Grätzel, *Science* **2016**, *354*, 206.
- [26] L. Kegelmann, P. Tockhorn, C. M. Wolff, J. A. Márquez, S. Caicedo-Dávila, L. Korte, T. Unold, W. Lövenich, D. Neher, B. Rech, S. Albrecht, *ACS Appl. Mater. Interfaces* **2019**, *11*, 9172.
- [27] D. Kiermasch, P. Rieder, K. Tvingstedt, A. Baumann, V. Dyakonov, *Sci. Rep.* **2016**, *6*, 39333.
- [28] C. M. Wolff, F. Zu, A. Paulke, L. P. Toro, N. Koch, D. Neher, *Adv. Mater.* **2017**, *29*, 1700159.
- [29] E. M. Hutter, J.-J. Hofman, M. L. Petrus, M. Moes, R. D. Abellón, P. Docampo, T. J. Savenije, *Adv. Energy Mater.* **2017**, *7*, 1602349.
- [30] J. Wang, W. Fu, S. Jariwala, I. Sinha, A. K.-Y. Jen, D. S. Ginger, *ACS Energy Lett.* **2019**, *4*, 222.

- [31] M. Stolterfoht, P. Caprioglio, C. M. Wolff, J. A. Márquez Prieto, J. Nordmann, S. Zhang, D. Rothhardt, U. Hörmann, Y. Amir, A. Redinger, L. Kegelmann, F. Zu, S. Albrecht, N. Koch, T. Kirchartz, M. Saliba, T. Unold, D. Neher, *Energy Environ. Sci.* **2019**, *12*, 2778.
- [32] P. Würfel, *Physics of Solar Cells: From Principles to New Concepts*, Wiley-VCH, Weinheim, Germany **2005**.
- [33] T. Kirchartz, J. Nelson, *Phys. Rev. B* **2012**, *86*, 165201.
- [34] K. Tvingstedt, L. Gil-Escrig, C. Momblona, P. Rieder, D. Kiermasch, M. Sessolo, A. Baumann, H. J. Bolink, V. Dyakonov, *ACS Energy Lett.* **2017**, *2*, 424.
- [35] G.-J. A. H. Wetzelaer, M. Scheepers, A. M. Sempere, C. Momblona, J. Ávila, H. J. Bolink, *Adv. Mater.* **2015**, *27*, 1837.
- [36] K. Tvingstedt, C. Deibel, *Adv. Energy Mater.* **2016**, *6*, 1502230.
- [37] C.-G. Wu, C.-H. Chiang, Z.-L. Tseng, M. K. Nazeeruddin, A. Hagfeldt, M. Grätzel, *Energy Environ. Sci.* **2015**, *8*, 2725.
- [38] C. Deibel, *Phys. Status Solidi A* **2009**, *206*.
- [39] S. D. Stranks, V. M. Burlakov, T. Leijtens, J. M. Ball, A. Gorieli, H. J. Snaith, *Phys. Rev. Appl.* **2014**, *2*, 34007.
- [40] T. S. Sherkar, C. Momblona, L. Gil-Escrig, H. J. Bolink, L. J. A. Koster, *Adv. Energy Mater.* **2017**, *7*, 1602432.
- [41] P. Caprioglio, M. Stolterfoht, C. M. Wolff, T. Unold, B. Rech, S. Albrecht, D. Neher, *Adv. Energy Mater.* **2019**, 1901631.
- [42] U. Würfel, L. Perdigón-Toro, J. Kurpiers, C. M. Wolff, P. Caprioglio, J. J. Rech, J. Zhu, X. Zhan, W. You, S. Shoaee, D. Neher, M. Stolterfoht, *J. Phys. Chem. Lett.* **2019**, *10*, 3473.
- [43] V. Sarritzu, N. Sestu, D. Marongiu, X. Chang, S. Masi, A. Rizzo, S. Colella, F. Quochi, M. Saba, A. Mura, G. Bongiovanni, *Sci. Rep.* **2017**, *7*, 44629.
- [44] D. Credgington, J. R. Durrant, *J. Phys. Chem. Lett.* **2012**, *3*, 1465.
- [45] A. Hofacker, D. Neher, *Phys. Rev. B* **2017**, *96*, 245204.
- [46] M. H. Futscher, J. M. Lee, L. McGovern, L. A. Muscarella, T. Wang, M. I. Haider, A. Fakhruddin, L. Schmidt-Mende, B. Ehrler, *Mater. Horiz.* **2019**.
- [47] P. Calado, D. Burkitt, J. Yao, J. Troughton, T. M. Watson, M. J. Carnie, A. M. Telford, B. C. O'Regan, J. Nelson, P. R. F. Barnes, *Phys. Rev. Appl.* **2019**, *11*, 044005.
- [48] A. Pockett, G. E. Eperon, T. Peltola, H. J. Snaith, A. Walker, L. M. Peter, P. J. Cameron, *J. Phys. Chem. C* **2015**, *119*, 3456.
- [49] I. Zarazua, G. Han, P. P. Boix, S. Mhaisalkar, F. Fabregat-Santiago, I. Mora-Seró, J. Bisquert, G. Garcia-Belmonte, *J. Phys. Chem. Lett.* **2016**, *7*, 5105.
- [50] A. Guerrero, G. Garcia-Belmonte, I. Mora-Sero, J. Bisquert, Y. S. Kang, T. J. Jacobsson, J. P. Correa-Baena, A. Hagfeldt, *J. Phys. Chem. C* **2016**, *120*, 8023.
- [51] V. Gonzalez-Pedro, E. J. Juarez-Perez, W. S. Arsyad, E. M. Barea, F. Fabregat-Santiago, I. Mora-Sero, J. Bisquert, *Nano Lett.* **2014**, *14*, 888.
- [52] D. Kiermasch, L. Gil-Escrig, A. Baumann, H. J. Bolink, V. Dyakonov, K. Tvingstedt, *J. Mater. Chem. A* **2019**, *7*, 14712.
- [53] S. Wheeler, D. Bryant, J. Troughton, T. Kirchartz, T. Watson, J. Nelson, J. R. Durrant, *J. Phys. Chem. C* **2017**, *121*, 13496.
- [54] H. Wang, A. Guerrero, A. Bou, A. M. Al-Mayouf, J. Bisquert, *Energy Environ. Sci.* **2019**.
- [55] D. Kiermasch, A. Baumann, M. Fischer, V. Dyakonov, K. Tvingstedt, *Energy Environ. Sci.* **2018**, *11*, 629.
- [56] A. Baumann, K. Tvingstedt, M. C. Heiber, S. Väh, C. Momblona, H. J. Bolink, V. Dyakonov, *APL Mater.* **2014**, *2*, 081501.
- [57] A. Paulke, S. D. Stranks, J. Knipert, J. Kurpiers, C. M. Wolff, N. Schön, H. J. Snaith, T. J. K. Brenner, D. Neher, *Appl. Phys. Lett.* **2016**, *108*, 113505.
- [58] C. Wehrenfennig, G. E. Eperon, M. B. Johnston, H. J. Snaith, L. M. Herz, *Adv. Mater.* **2014**, *26*, 1584.
- [59] W.-A. Quitsch, D. W. deQuilettes, O. Pflingsten, A. Schmitz, S. Ognjanovic, S. Jariwala, S. Koch, M. Winterer, D. S. Ginger, G. Bacher, *J. Phys. Chem. Lett.* **2018**, *9*, 2062.
- [60] A. Merdasa, A. Kiligaridis, C. Rehermann, M. Abdi-Jalebi, J. Stöber, B. Louis, M. Gerhard, S. D. Stranks, E. L. Unger, I. G. Scheblykin, *ACS Energy Lett.* **2019**, *4*, 1370.
- [61] L. G. Kudriashova, D. Kiermasch, P. Rieder, M. Campbell, K. Tvingstedt, A. Baumann, G. V. Astakhov, V. Dyakonov, *J. Phys. Chem. Lett.* **2017**, *8*, 4698.
- [62] D. W. deQuilettes, W. Zhang, V. M. Burlakov, D. J. Graham, T. Leijtens, A. Osherov, V. Bulović, H. J. Snaith, D. S. Ginger, S. D. Stranks, *Nat. Commun.* **2016**, *7*, 11683.
- [63] T. Unold, L. Gütay, *Advanced Characterization Techniques for Thin Film Solar Cells*, Wiley-VCH, Weinheim, Germany **2011**, pp. 151–175.
- [64] I. L. Braly, H. W. Hillhouse, *J. Phys. Chem. C* **2016**, *120*, 893.
- [65] N. Wu, Y. Wu, D. Walter, H. Shen, T. Duong, D. Grant, C. Barugkin, X. Fu, J. Peng, T. White, K. Catchpole, K. Weber, *Energy Technol.* **2017**, *5*, 1827.
- [66] G. El-Hajje, C. Momblona, L. Gil-Escrig, J. Ávila, T. Guillemot, J.-F. F. Guillemoles, M. Sessolo, H. J. Bolink, L. Lombez, *Energy Environ. Sci.* **2016**, *9*, 2286.
- [67] P. Würfel, *J. Phys. C: Solid State Phys.* **1982**, *15*, 3967.
- [68] U. Rau, *Phys. Rev. B* **2007**, *76*, 085303.
- [69] T. Kirchartz, J. Nelson, U. Rau, *Phys. Rev. Appl.* **2016**, *5*, 054003.
- [70] C. Donolato, *Appl. Phys. Lett.* **1985**, *46*, 270.
- [71] Z. Liu, L. Krückemeier, B. Krogmeier, B. Klingebiel, J. A. Márquez, S. Levchenko, S. Öz, S. Mathur, U. Rau, T. Unold, T. Kirchartz, *ACS Energy Lett.* **2018**, *4*, 110.
- [72] P. Caprioglio, F. Zu, C. M. Wolff, J. A. Márquez Prieto, M. Stolterfoht, P. Becker, N. Koch, T. Unold, B. Rech, S. Albrecht, D. Neher, *Sustainable Energy Fuels* **2019**, *3*, 550.
- [73] S. Yang, J. Dai, Z. Yu, Y. Shao, Y. Zhou, X. Xiao, X. C. Zeng, J. Huang, *J. Am. Chem. Soc.* **2019**, *141*, 5781.
- [74] M. Saliba, *Adv. Energy Mater.* **2019**, *9*, 1803754.
- [75] P. Fassl, V. Lami, A. Bausch, Z. Wang, M. T. Klug, H. J. Snaith, Y. Vaynzof, *Energy Environ. Sci.* **2018**, *11*, 3380.
- [76] P. Becker, J. A. Márquez, J. Just, A. Al-Ashouri, C. Hages, H. Hempel, M. Jošt, S. Albrecht, R. Frahm, T. Unold, *Adv. Energy Mater.* **2019**, *9*, 1900555.
- [77] S. Braunger, L. E. Mundt, C. M. Wolff, M. Mews, C. Rehermann, M. Jošt, A. Tejada, D. Eisenhauer, C. Becker, J. A. Guerra, E. Unger, L. Korte, D. Neher, M. C. Schubert, B. Rech, S. Albrecht, *J. Phys. Chem. C* **2018**, *122*, 17123.
- [78] A. Cabas-Vidani, S. G. Haass, C. Andres, R. Caballero, R. Figi, C. Schreiner, J. A. Márquez, C. Hages, T. Unold, D. Bleiner, A. N. Tiwari, Y. E. Romanyuk, *Adv. Energy Mater.* **2018**, *8*, 1801191.
- [79] J. Márquez, H. Stange, C. J. Hages, N. Schaefer, S. Levchenko, S. Giraldo, E. Saucedo, K. Schwarzburg, D. Abou-Ras, A. Redinger, M. Klaus, C. Genzel, T. Unold, R. Mainz, *Chem. Mater.* **2017**, *29*, 9399.
- [80] S. Levchenko, J. Just, A. Redinger, G. Larramona, S. Bourdais, G. Dennler, A. Jacob, T. Unold, *Phys. Rev. Appl.* **2016**, *5*, 024004.
- [81] M. A. Green, A. W. Y. Ho-Baillie, *ACS Energy Lett.* **2019**, *4*, 1639.
- [82] J. Benduhn, K. Tvingstedt, F. Piersimoni, S. Ullbrich, Y. Fan, M. Tropicano, K. A. McGarry, O. Zeika, M. K. Riede, C. J. Douglas, S. Barlow, S. R. Marder, D. Neher, D. Spoltore, K. Vandewal, *Nat. Energy* **2017**, *2*, 17053.
- [83] D. Guo, V. M. Caselli, E. M. Hutter, T. J. Savenije, *ACS Energy Lett.* **2019**, *4*, 855.
- [84] S. Zhang, S. M. Hosseini, R. Gunder, A. Petsiuk, P. Caprioglio, C. M. Wolff, S. Shoaee, P. Meredith, S. Schorr, T. Unold, P. L. Burn, D. Neher, M. Stolterfoht, *Adv. Mater.* **2019**, *31*, 1901090.
- [85] E. Yablonovitch, Lecture Series: Stanford University for EE 237 Solar Energy Conversion by Dr. Aneesh Nainani, **2013**.

- [86] K. Tvingstedt, O. Malinkiewicz, A. Baumann, C. Deibel, H. J. Snaith, V. Dyakonov, H. J. Bolink, *Sci. Rep.* **2015**, *4*, 6071.
- [87] Y. Hou, W. Chen, D. Baran, T. Stubhan, N. A. Luechinger, B. Hartmeier, M. Richter, J. Min, S. Chen, C. O. R. Quiroz, N. Li, H. Zhang, T. Heumueller, G. J. Matt, A. Osvet, K. Forberich, Z.-G. Zhang, Y. Li, B. Winter, P. Schweizer, E. Spiecker, C. J. Brabec, *Adv. Mater.* **2016**, *28*, 5112.
- [88] W. Tress, N. Marinova, O. Inganäs, M. K. Nazeeruddin, S. M. Zakeeruddin, M. Graetzel, *Adv. Energy Mater.* **2015**, *5*, 1400812.
- [89] F. Staub, H. Hempel, J.-C. Hebig, J. Mock, U. W. Paetzold, U. Rau, T. Unold, T. Kirchartz, *Phys. Rev. Appl.* **2016**, *6*, 044017.
- [90] B. Krogmeier, F. Staub, D. Grabowski, U. Rau, T. Kirchartz, *Sustainable Energy Fuels* **2018**, *2*, 1027.
- [91] L. Kegelmann, C. M. Wolff, C. Awino, F. Lang, E. L. Unger, L. Korte, T. Dittrich, D. Neher, B. Rech, S. Albrecht, *ACS Appl. Mater. Interfaces* **2017**, *9*, 17245.
- [92] G. Grancini, D. Viola, Y. Lee, M. Saliba, S. Paek, K. T. Cho, S. Orlandi, M. Cavazzini, F. Fungo, M. I. Hossain, A. Belaidi, N. Tabet, G. Pozzi, G. Cerullo, M. K. Nazeeruddin, *ChemPhysChem* **2017**, *18*, 2381.
- [93] J. Horn, I. Minda, H. Schwoerer, D. Schlottwein, *Phys. Status Solidi Basic Res.* **2019**, *256*, 1.
- [94] C. S. Ponceca Jr., V. Sundström, *Nanoscale* **2016**, *8*, 6249.
- [95] Q. Wang, E. Mosconi, C. Wolff, J. Li, D. Neher, F. De Angelis, G. P. Suranna, R. Grisorio, A. Abate, *Adv. Energy Mater.* **2019**, *9*, 1900990.
- [96] B. Krogmeier, F. Staub, D. Grabowski, U. Rau, T. Kirchartz, *Sustainable Energy Fuels* **2018**, *1*.
- [97] T. Kirchartz, L. Krückemeier, E. L. Unger, *APL Mater.* **2018**, *6*, 100702.
- [98] T. J. Savenije, A. J. Ferguson, N. Kopidakis, G. Rumbles, *J. Phys. Chem. C* **2013**, *117*, 24085.
- [99] M. B. Price, J. Butkus, T. C. Jellicoe, A. Sadhanala, A. Briane, J. E. Halpert, K. Broch, J. M. Hodgkiss, R. H. Friend, F. Deschler, *Nat. Commun.* **2015**, *6*, 8420.
- [100] P. Piatkowski, B. Cohen, F. J. Ramos, M. R. Di Nunzio, M. K. Nazeeruddin, M. Grätzel, S. Ahmad, A. Douhal, *Phys. Chem. Chem. Phys.* **2015**, *17*, 14674.
- [101] A. Spies, M. List, T. Sarkar, U. Würfel, *Adv. Energy Mater.* **2017**, *7*, 1601750.
- [102] P. Schulz, E. Edri, S. Kirmayer, G. Hodes, D. Cahen, A. Kahn, *Energy Environ. Sci.* **2014**, *7*, 1377.
- [103] L. E. Polander, P. Pahnner, M. Schwarze, M. Saalfrank, C. Koerner, K. Leo, *APL Mater.* **2014**, *2*, 081503.
- [104] Q. Wang, Y. Shao, Q. Dong, Z. Xiao, Y. Yuan, J. Huang, *Energy Environ. Sci.* **2014**, *7*, 2359.
- [105] C.-G. Wu, C.-H. Chiang, S. H. Chang, *Nanoscale* **2016**, *8*, 4077.
- [106] Q. Lin, A. Armin, R. C. R. Nagiri, P. L. Burn, P. Meredith, *Nat. Photonics* **2015**, *9*, 106.
- [107] A. Rajagopal, P.-W. Liang, C.-C. Chueh, Z. Yang, A. K.-Y. Jen, *ACS Energy Lett.* **2017**, *2*, 2531.
- [108] N. J. Jeon, H. Na, E. H. Jung, T.-Y. Yang, Y. G. Lee, G. Kim, H.-W. Shin, S. I. Seok, J. Lee, J. Seo, *Nat. Energy* **2018**, *3*, 682.
- [109] R. A. Belisle, P. Jain, R. Prasanna, T. Leijtens, M. D. McGehee, *ACS Energy Lett.* **2016**, *1*, 556.
- [110] P.-W. Liang, C.-C. Chueh, S. T. Williams, A. K.-Y. Jen, *Adv. Energy Mater.* **2015**, *5*, 1402321.
- [111] C. Bi, Y. Yuan, Y. Fang, J. Huang, *Adv. Energy Mater.* **2015**, *5*, 1401616.
- [112] F. Zu, P. Amsalem, D. A. Egger, R. Wang, C. M. Wolff, H. Fang, M. A. Loi, D. Neher, L. Kronik, S. Duhm, N. Koch, *J. Phys. Chem. Lett.* **2019**, *10*, 601.
- [113] F. S. Zu, P. Amsalem, I. Salzmann, R. Bin Wang, M. Ralaiarisoa, S. Kowarik, S. Duhm, N. Koch, *Adv. Opt. Mater.* **2017**, *5*, 1700139.
- [114] F. Zu, C. M. Wolff, M. Ralaiarisoa, P. Amsalem, D. Neher, N. Koch, *ACS Appl. Mater. Interfaces* **2019**, *11*, 21578.
- [115] I. M. Hermes, Y. Hou, V. W. Bergmann, C. J. Brabec, S. A. L. Weber, *J. Phys. Chem. Lett.* **2018**, *9*, 6249.
- [116] S. A. L. Weber, I. M. Hermes, S. H. Turren-Cruz, C. Gort, V. W. Bergmann, L. Gilson, A. Hagfeldt, M. Graetzel, W. Tress, R. Berger, *Energy Environ. Sci.* **2018**, *11*, 2404.
- [117] A. Rajagopal, R. J. Stoddard, S. B. Jo, H. W. Hillhouse, A. K. Y. Jen, *Nano Lett.* **2018**, *18*, 3985.
- [118] J. Peng, J. I. Khan, W. Liu, E. Ugur, T. Duong, Y. Wu, H. Shen, K. Wang, H. Dang, E. Aydin, X. Yang, Y. Wan, K. J. Weber, K. R. Catchpole, F. Laquai, S. De Wolf, T. P. White, *Adv. Energy Mater.* **2018**, *8*, 1801208.
- [119] Q. Wang, Q. Dong, T. Li, A. Gruverman, J. Huang, *Adv. Mater.* **2016**, *28*, 6734.
- [120] J.-P. Correa-Baena, W. Tress, K. Domanski, E. H. Anaraki, S.-H. Turren-Cruz, B. Roose, P. P. Boix, M. Grätzel, M. Saliba, A. Abate, A. Hagfeldt, *Energy Environ. Sci.* **2017**, *10*, 1207.
- [121] S.-H. Turren-Cruz, A. Hagfeldt, M. Saliba, *Science* **2018**, *362*, 449.
- [122] Q. Jiang, Y. Zhao, X. Zhang, X. Yang, Y. Chen, Z. Chu, Q. Ye, X. Li, Z. Yin, J. You, *Nat. Photonics* **2019**.
- [123] K. T. Cho, S. Paek, G. Grancini, C. Roldán-Carmona, P. Gao, Y. Lee, M. K. Nazeeruddin, *Energy Environ. Sci.* **2017**, *10*, 621.
- [124] C. Momblona, L. Gil-Escrig, E. Bandiello, E. M. Hutter, M. Sessolo, K. Lederer, J. Blochwitz-Nimoth, H. J. Bolink, *Energy Environ. Sci.* **2016**, *9*, 3456.
- [125] S. S. Shin, E. J. Yeom, W. S. Yang, S. Hur, M. G. Kim, J. Im, J. Seo, J. H. Noh, S. I. Seok, *Science* **2017**, *356*, 167.
- [126] Y. Shao, Y. Yuan, J. Huang, *Nat. Energy* **2016**, *1*, 15001.
- [127] J. Zhao, X. Zheng, Y. Deng, T. Li, Y. Shao, A. Gruverman, J. Shield, J. Huang, *Energy Environ. Sci.* **2016**, *9*, 3650.
- [128] J. T.-W. Wang, Z. Wang, S. Pathak, W. Zhang, D. W. DeQuilettes, F. Wisnivesky-Rocca-Rivarola, J. Huang, P. K. Nayak, J. B. Patel, H. A. Mohd Yusof, Y. Vaynzof, R. Zhu, I. Ramirez, J. Zhang, C. Ducati, C. Grovenor, M. B. Johnston, D. S. Ginger, R. J. Nicholas, H. J. Snaith, *Energy Environ. Sci.* **2016**, *9*, 2892.
- [129] D. Bi, X. Li, J. V. Milić, D. J. Kubicki, N. Pellet, J. Luo, T. LaGrange, P. Mettraux, L. Emsley, S. M. Zakeeruddin, M. Grätzel, *Nat. Commun.* **2018**, *9*, 4482.
- [130] M. Jošt, S. Albrecht, L. Kegelmann, C. M. Wolff, F. Lang, B. Lipovšek, J. Krč, L. Korte, D. Neher, B. Rech, M. Topič, *ACS Photonics* **2017**, *4*, 1232.
- [131] J. M. Richter, M. Abdi-Jalebi, A. Sadhanala, M. Tabachnyk, J. P. H. Rivett, L. M. Pazos-Outón, K. C. Gödel, M. Price, F. Deschler, R. H. Friend, *Nat. Commun.* **2016**, *7*, 13941.
- [132] L. M. Pazos-Outón, M. Szumilo, R. Lamboll, J. M. Richter, M. Crespo-Quesada, M. Abdi-Jalebi, H. J. Beeson, M. Vru ini, M. Alsari, H. J. Snaith, B. Ehrler, R. H. Friend, F. Deschler, *Science* **2016**, *351*, 1430.
- [133] M. A. Green, *Prog. Photovoltaics* **2012**, *20*, 472.
- [134] O. D. Miller, E. Yablonovitch, S. R. Kurtz, *IEEE J. Photovoltaics* **2012**, *2*, 303.
- [135] E. D. Kosten, J. H. Atwater, J. Parsons, A. Polman, H. A. Atwater, *Light: Sci. Appl.* **2013**, *2*, e45.
- [136] F. Staub, T. Kirchartz, K. Bittkau, U. Rau, *J. Phys. Chem. Lett.* **2017**, *8*, 5084.
- [137] Y. Cao, N. Wang, H. Tian, J. Guo, Y. Wei, H. Chen, Y. Miao, W. Zou, K. Pan, Y. He, H. Cao, Y. Ke, M. Xu, Y. Wang, M. Yang, K. Du, Z. Fu, D. Kong, D. Dai, Y. Jin, G. Li, H. Li, Q. Peng, J. Wang, W. Huang, *Nature* **2018**, *562*, 249.